The Pennsylvania State University

The Graduate School

BISMUTH ZINC NIOBATE FILMS FOR DIELECTRIC APPLICATIONS

A Thesis in

Materials Science and Engineering

by

Ryan Lewis Thayer

©2002 Ryan Lewis Thayer

Submitted in Partial Fulfillment
of the Requirements
for the Degree of

Master of Science

December 2002

I grant The Pennsylvania State University the non-exclusive right to use this work for the University's own purposes and to make single copies of the work available to the public on a not-for-profit basis if copies are not otherwise available.

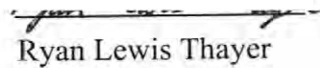

Ryan Lewis Thayer

We approve the thesis of Ryan Lewis Thayer.

Date of Signature

7/31/02

Susan Trolier-McKinstry
Professor of Ceramic Science and Engineering
Thesis Co-Advisor

7/15/02

Clive A. Randall
Professor of Materials Science and Engineering
Thesis Co-Advisor

7/15/02

Thomas R. Shrout
Professor of Materials and Senior Scientist

July 23, 2002

Thomas N. Jackson
Professor of Electrical Engineering

7/23/02

James P. Runt
Professor of Polymer Science
Coordinator of Graduate Program, Department of Materials Science and Engineering

ABSTRACT

In this thesis, three compositions of Bi-Zn-Nb (BZN) thin films were studied: $Bi_{1.5}Zn_{1.0}Nb_{1.5}O_7$, $Bi_{1.5}Zn_{0.5}Nb_{1.5}O_{6.5}$, and $Bi_2Zn_{2/3}Nb_{4/3}O_7$. It was found that $Bi_{1.5}Zn_{0.5}Nb_{1.5}O_{6.5}$ has the cubic pyrochlore structure, a relative permittivity ~180 and loss tangent < 0.005 (Q>200) when processed at 600 – 650 °C, and a temperature coefficient of capacitance (TCC) of –275 ppm/°C when processed at 650 °C, measured at 10 kHz.

The thickness-dependence of dielectric properties of $Bi_{1.5}Zn_{1.0}Nb_{1.5}O_7$ films was studied. It was found that for thicknesses > 520 Angstroms, $Bi_{1.5}Zn_{1.0}Nb_{1.5}O_7$ has thickness-independent permittivity, dc field tunability, and leakage.

Cubic $Bi_{1.5}Zn_{0.5}Nb_{1.5}O_{6.5}$ shows a similar dielectric relaxation as has previously been observed in cubic $Bi_{1.5}Zn_{1.0}Nb_{1.5}O_7$, although the onset of relaxation occurred ~30-50 K lower for $Bi_{1.5}Zn_{0.5}Nb_{1.5}O_{6.5}$. This lower onset temperature is important for applications since higher frequencies can be reached without the shoulder in the loss tangent peak lowering the electrical quality factor. The activation energy and jump frequency for $Bi_{1.5}Zn_{0.5}Nb_{1.5}O_{6.5}$ were calculated to be 0.11 ± 0.0054 eV and 4.57 x 10^{12} ± 2.86 Hz, respectively, using the Arrhenius equation.

$Bi_{1.5}Zn_{1.0}Nb_{1.5}O_7$ and $Bi_{1.5}Zn_{0.5}Nb_{1.5}O_{6.5}$ show similar tunability of the permittivity under dc field (26 % at 1.8 MV/cm). Also, $Bi_{1.5}Zn_{1.0}Nb_{1.5}O_7$ shows 45 % tunability at 3.0 MV/cm, and $Bi_2Zn_{2/3}Nb_{4/3}O_7$ has 20 % maximum tunability at 4.0 MV/cm.

It was found that BZN films are also tunable with ac electric fields. The permittivity of $Bi_2Zn_{2/3}Nb_{4/3}O_7$ increased <1 % at 500 kV/cm, and 6 % for $Bi_{1.5}Zn_{0.5}Nb_{1.5}O_{6.5}$ at 500 kV/cm. Since the permittivity of BZN films increases with ac field but decreases with dc field, it was concluded that different mechanisms were responsible for tunability under ac and dc fields.

Leakage currents of BZN films were also measured. It was found that $Bi_{1.5}Zn_{1.0}Nb_{1.5}O_7$ and $Bi_{1.5}Zn_{0.5}Nb_{1.5}O_{6.5}$ have low leakage. In addition, it was found that the leakage behavior of BZN films shows a dependence on the electrode materials used.

TABLE OF CONTENTS

LIST OF FIGURES...vii

LIST OF TABLES...x

Chapter 1 POTENTIAL USES OF BISMUTH ZINC NIOBATE FILMS...1

1.1 Bulk BZN...3
1.2 BZN Thin Films...7
1.3 Dipole Glasses...11
1.4 Ferroelectric Relaxors...12
1.5 Models of Relaxor Ferroelectrics...13
1.5.1 Superparaelectric Model...13
1.5.2 Glassy Model...14
1.5.3 Models Incorporating Random Fields...16
1.5.4 Breathing Model...18
1.6 Thesis Objectives...20
1.7 References...21

Chapter 2 EXPERIMENTAL PROCEDURE...27

2.1 Solution Preparation...27
2.2 Thin Film Deposition...28
2.3 Characterization...29
2.4 References...32

Chapter 3 RESULTS...33

3.1 Low Field: $Bi_{1.5}Zn_{1.0}Nb_{1.5}O_7$...33
3.2 A New Cubic Composition: $Bi_{1.5}Zn_{0.5}Nb_{1.5}O_{6.5}$...37
3.2.1 Thermal Analysis...38
3.2.2 Crystallization...38
3.2.3 Low Field: $Bi_{1.5}Zn_{0.5}Nb_{1.5}O_{6.5}$...39
3.3 High dc Field...44

3.3.1 High dc Field: $Bi_{1.5}Zn_{1.0}Nb_{1.5}O_7$....44
3.3.2 High dc Field: $Bi_{1.5}Zn_{0.5}Nb_{1.5}O_{6.5}$....47
3.3.3 High dc Field: $Bi_2Zn_{2/3}Nb_{4/3}O_7$....49
3.3.4 Polarization-Field Measurements....51
3.4 ac Field Tunability of BZN....52
3.5 Leakage Current....54
3.5.1 Leakage Current: Background....55
3.5.2 Leakage Current: $Bi_{1.5}Zn_{1.0}Nb_{1.5}O_7$....59
3.5.3 Leakage Current: $Bi_{1.5}Zn_{0.5}Nb_{1.5}O_{6.5}$....63
3.6 References....64

Chapter 4: SUMMARY AND FUTURE WORK....69

4.1 Summary....69
4.2 Future Work....75
4.3 References....79

LIST OF FIGURES

Figure 1-1: Crystal structure of $Bi_{1.5}Zn_{1.0}Nb_{1.5}O_7$.[25] 4

Figure 1-2: Crystal structure of $Bi_2Zn_{2/3}Nb_{4/3}O_7$.[27] (a) Side view, (b) Top view..........4

Figure 1-3: XRD pattern of bulk $Bi_{1.5}Zn_{1.0}Nb_{1.5}O_7$, with BZN peaks indicated by * and arrows indicating positions of ZnO peaks. (Courtesy of Dr. Igor Levin, NIST)....6

Figure 1-4: X-Ray Diffraction (XRD) patterns showing structure of BZN thin films as a function of firing temperature. (a) $Bi_{1.5}Zn_{1.0}Nb_{1.5}O_7$, (b) $Bi_2Zn_{2/3}Nb_{4/3}O_7$[15] 9

Figure 1-5: Permittivity and loss of BZN thin films as a function of applied dc field. (a) $Bi_{1.5}Zn_{1.0}Nb_{1.5}O_7$, (b) $Bi_2Zn_{2/3}Nb_{4/3}O_7$[15] 10

Figure 1-6: Measuring temperature dependence of permittivity and loss tangent of $Bi_{1.5}Zn_{1.0}Nb_{1.5}O_7$ fired at 750 °C[15] 10

Figure 3-1: Relative permittivity and loss tangent of $Bi_{1.5}Zn_{1.0}Nb_{1.5}O_7$ films as a function of firing temperature, measured at 10 kHz and 0.03 V ac. Typical film thickness = 0.4 μm....................................34

Figure 3-2: Inverse capacitance vs. thickness for $Bi_{1.5}Zn_{1.0}Nb_{1.5}O_7$....................................35

Figure 3-3: Permittivity vs. dc field for $(Ba_{0.7}Sr_{0.3})Ti_{0.53}O_3$ films, with thicknesses of 15 – 600 nm. The thin films were deposited using MOCVD.[4] 36

Figure 3-4: Equivalent oxide thickness for $Bi_{1.5}Zn_{1.0}Nb_{1.5}O_7$ films........................37

Figure 3-5: DTA curve of $Bi_{1.5}Zn_{0.5}Nb_{1.5}O_{6.5}$ MOD solution....................................38

Figure 3-6: XRD patterns of $Bi_{1.5}Zn_{0.5}Nb_{1.5}O_{6.5}$ films fired at different temperatures....39

Figure 3-7: Relative permittivity and loss tangent of BZN films at different firing temperatures, measured at 10 kHz and 0.03 V ac....................................40

Figure 3-8: TCC of BZN films at different firing temperatures....................................41

Figure 3-9: (a) Permittivity and (b) loss of $Bi_{1.5}Zn_{0.5}Nb_{1.5}O_{6.5}$ films (fired at 600 °C) and $Bi_{1.5}Zn_{1.0}Nb_{1.5}O_7$ films (fired at 750 °C) as a function of measuring temperature. For each composition, the frequency changes from the top curve to bottom curve in the order: 0.5, 1, 5, 10, 50, 100 kHz for permittivity; 10, 5, 1 kHz for the loss tangent....................................42

Figure 3-10: Arrhenius plot of $Bi_{1.5}Zn_{0.5}Nb_{1.5}O_{6.5}$ based on curve-fit data in Figure 3-9b....43

Figure 3-11: Permittivity and loss tangent of $Bi_{1.5}Zn_{1.0}Nb_{1.5}O_7$ as a function of applied dc field, measured at 10 kHz and 0.03 V ac. (a) 300 K, (b) 77 K....45

Figure 3-12: Permittivity of $Bi_{1.5}Zn_{1.0}Nb_{1.5}O_7$ with applied dc field for varying thicknesses of films with Cr/Au top electrodes, measured at 10 kHz, 0.03 V ac, and 77 K. Loss tangent ≤ 0.04....46

Figure 3-13: Permittivity and loss tangent of $Bi_{1.5}Zn_{0.5}Nb_{1.5}O_{6.5}$ films as a function of applied dc field, measured at 10 kHz, 0.03 V ac, and 77 K....48

Figure 3-14: Plots of capacitance density vs. thickness of films comparing $Bi_{1.5}Zn_{1.0}Nb_{1.5}O_7$, $Bi_{1.5}Zn_{0.5}Nb_{1.5}O_{6.5}$, and $(Ba_{0.7}Sr_{0.3})Ti_{0.53}O_3$ (BZN-1, BZN-0.5, and BST, respectively). (a) 1 V dc applied, (b) 5 V dc applied....49

Figure 3-15: Permittivity and loss tangent of $Bi_2Zn_{2/3}Nb_{4/3}O_7$ as a function of applied dc field, measured at 10 kHz, 0.03 V ac, and 77 K....50

Figure 3-16: P-E curves for $Bi_{1.5}Zn_{1.0}Nb_{1.5}O_7$, showing both measured and integrated C-E data from Figure 3-11b, 77 K....51

Figure 3-17: P-E curves for $Bi_2Zn_{2/3}Nb_{4/3}O_7$, showing both measured and integrated C-E data from Figure 3-14, 77 K....52

Figure 3-18: Permittivity and loss tangent of $Bi_2Zn_{2/3}Nb_{4/3}O_7$ films as a function of applied ac field, measured at 10 kHz, 300 K....53

Figure 3-19 Permittivity and loss tangent of $Bi_{1.5}Zn_{0.5}Nb_{1.5}O_{6.5}$ films as a function of applied ac field, measured at 10 kHz. (a) 77 K, (b) 300 K....53

Figure 3-20: Schematic of tunneling conduction mechanism[20]....56

Figure 3-21: (a) Space charge limited, and (b) Poole-Frenkel mechanisms of conduction[20]....57

Figure 3-22: Schematic of Schottky emission conduction mechanism[20]....59

Figure 3-23: Plot of leakage current vs. dc field of samples with either Pt or Cr/Au top electrodes....60

Figure 3-24: Plot of leakage current as a function of applied dc field for 120 nm $Bi_{1.5}Zn_{1.0}Nb_{1.5}O_7$ film with Cr/Au top electrodes....61

Figure 3-25: Leakage current of varying thicknesses of $Bi_{1.5}Zn_{1.0}Nb_{1.5}O_7$ films with Cr/Au top electrodes, as a function of applied dc field....................................62

Figure 3-26: Leakage current of $Bi_{1.5}Zn_{0.5}Nb_{1.5}O_{6.5}$ film as a function of applied dc field; Pt top electrodes..63

Figure 4-1: Ternary composition diagram for the Bi_2O_3 – ZnO – Nb_2O_5 system. Also shown is the tie line relating ZnO, $Bi_{1.5}Zn_{1.0}Nb_{1.5}O_7$, $Bi_{1.5}Zn_{0.5}Nb_{1.5}O_{6.5}$, and $BiNbO_4$..70

Figure 4-2a: A possible phase diagram for the BZN system combining experimentally determined thin film and ceramic data..72

Figure 4-2b: A possible phase diagram for the BZN system combining experimentally determined thin film and ceramic data..73

LIST OF TABLES

Table 4-1: Summary of dielectric properties and processing temperatures for three compositions of BZN, comparing thin film and ceramics. Note that $Bi_{1.5}Zn_{0.5}Nb_{1.5}O_{6.5}$ ceramic samples were not prepared.[2] 71

Chapter 1

POTENTIAL USES OF BISMUTH ZINC NIOBATE FILMS

The purpose of this research is to study Bi_2O_3-ZnO-Nb_2O_5 (BZN) thin films that can be used for a variety of electronic applications. Applications for microwave devices operating at wavelengths ranging from 0.3 to 30 cm, corresponding to frequencies of 1 to 100 GHz include radar, communications, radiometry, medicine, physics, and chemistry.[1] Currently, there is a need for low processing temperature materials for high frequency applications.[2] A low processing temperature would reduce processing costs and also allow for simultaneous processing with other components. In addition, a moderately high permittivity and high Q are important ($Q=\frac{1}{\tan\delta}$).[3] The dielectric properties of the material must also be stable over the temperature range which a specific application's operating environment demands. In bulk form, BZN is a candidate for applications that require low processing temperature which operate at high frequencies. More is known about bulk BZN since it has been studied for decoupling capacitor applications,[3-9] but relatively little is known about BZN films.

A potential application of BZN thin films is on-chip decoupling capacitors. As system clock speeds increase, decoupling capacitors are needed to minimize line

inductances and switching noise in the integrated circuits (ICs).[3] The effectiveness of power distribution systems in digital circuitry is reduced by the increasing clock speeds and the growing number of functions that simultaneously occur in an IC.[10] Switching noise is described as voltage fluctuations that result from the effective inductance of the chip and package.[11] Switching noise reduces the reliability and performance of the IC in three ways: (1) off-chip delays increase due to a distortion of the output from the active drivers,[12] (2) logic errors or a loss of data integrity can result from voltage fluctuations,[12] and (3) electromagnetic interference (EMI) in the system can result.[13]

Switching noise can be reduced using a decoupling capacitor that stores an electrical charge that can be released into the circuits to reduce the impact of voltage fluctuations in the power distribution network. However, the instantaneous delivery of current can be hindered by the inductance of the power supply and distribution lines.[14] This inductance can be greatly reduced by using on-chip decoupling capacitors.[10] This would eliminate the leads and connections that contribute to inductance, and therefore more effectively reduce high frequency noise.[11] An important requirement for an on-chip decoupling capacitor is a high permittivity thin film dielectric with a high Q at the operating clock speed of an IC,[11] currently on the order of 1-10 GHz. This requirement makes it difficult to use ferroelectric materials, because at microwave frequencies domain wall oscillations contribute to higher losses, leading to a $Q < 200$.[1]

In addition to reduced switching noise, other advantages of on-chip capacitors compared to off-chip include faster response and the possibility of simultaneous processing with the integrated circuit itself. Processing the capacitor on-chip would

require the maximum temperatures be comparable to that used for the back-end processes (~ 400 °C), to avoid degradation of the circuit itself. These low processing temperatures eliminate many potential candidates, including most ferroelectric films.[2]

Because the dielectric properties of BZN thin films are similar to those of bulk materials,[15] this chapter begins with an introduction to bulk bismuth pyrochlores.

1.1 Bulk BZN

Bulk bismuth-based pyrochlore systems have been studied by several researchers, especially the BZN pyrochlore system.[3-9,16-27] Cubic pyrochlores have the general formula $A_2B_2O_6O'$ and are considered to be a derivative of the fluorite structure AO_2 where the unit cell is doubled and the A site is split into both A and B sites.[19] The larger A cations are eightfold coordinated with oxygen[28] yielding distorted cubes. The smaller B cations are sixfold coordinated with oxygen, yielding distorted octahedras.[28] One of the seven oxygens is only bonded to A cations.[3]

There are 2 main phases in the system, a cubic pyrochlore phase with space group Fd3m (Figure 1-1), and a monoclinic zirconolite phase with space group C2/c which has been described as a derivative of the pyrochlore structure[27] (Figure 1-2). According to structural refinements using neutron diffraction data from $Bi_2Zn_{2/3}Nb_{4/3}O_7$, Nb preferentially occupies six-fold coordinated sites in octahedral sheets parallel to the (001) planes, while Zn is distributed between two five-fold coordinated sites near the centers of the six-membered rings of $[Nb(Zn)O_6]$ octahedra.[27] The Nb/Zn cation layers alternate along the *c*-axis with Bi-layers.

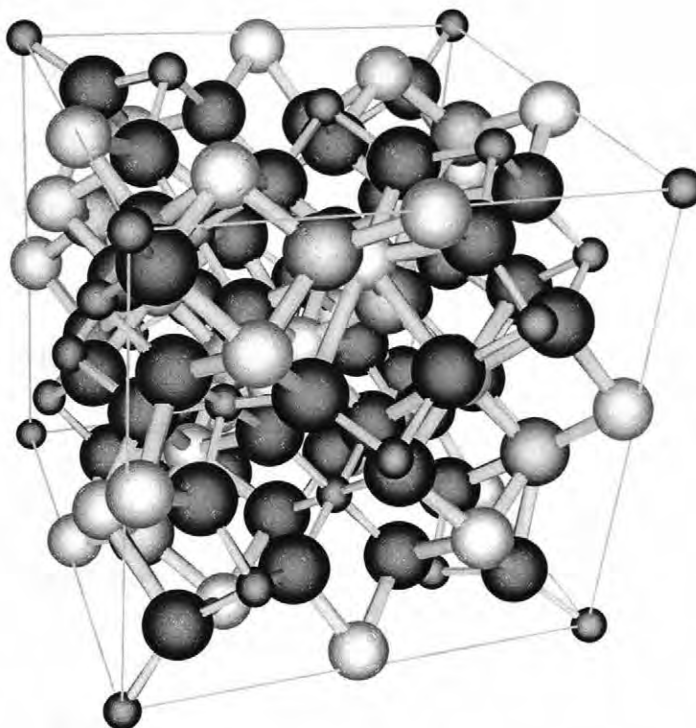

Figure 1-1: Crystal structure of $Bi_{1.5}Zn_{1.0}Nb_{1.5}O_7$.[25]

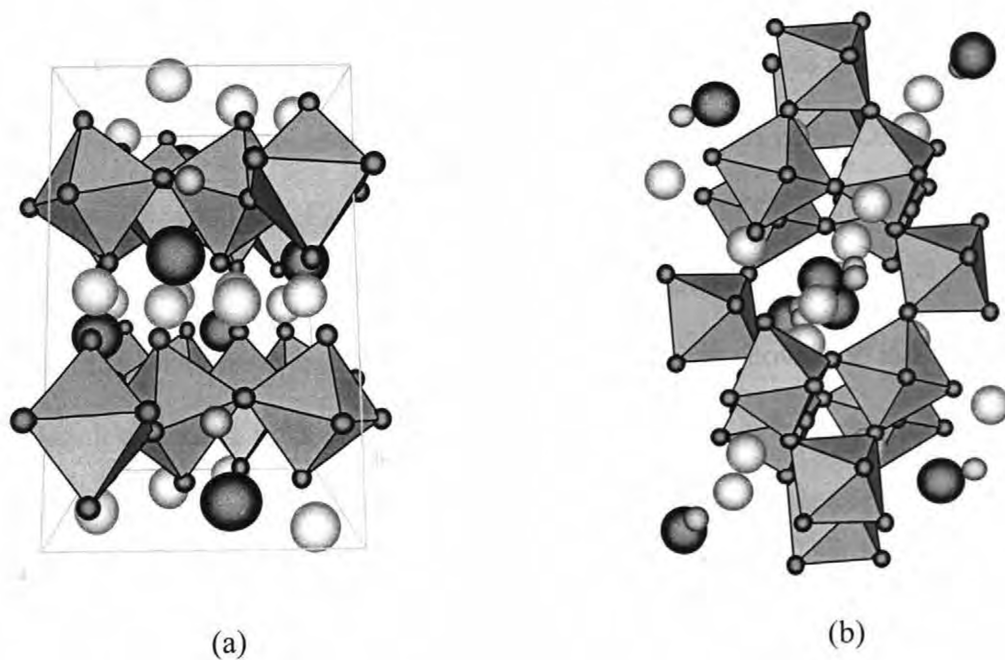

(a) (b)

Figure 1-2: Crystal structure of $Bi_2Zn_{2/3}Nb_{4/3}O_7$.[27] (a) Side view, (b) Top view.

Although there is a correlation between ionic radii of cations and the stabilization of the pyrochlore structure, other factors such as the electronegativity of cations, charge neutrality, and the thermodynamic stability of competitive phases are also important. With this in mind, the formation of the pyrochlore structure can be examined in terms of the ratio of the radii of cations (r_A/r_B). Subramanian et al. gave the radius ratio limits of pyrochlore as $1.46 < r_A/r_B < 1.80$ Angstroms and $1.4 < r_A/r_B < 2.2$ Angstroms, respectively for $A_2^{3+}B_2^{4+}O_7$ and $A_2^{2+}B_2^{5+}O_7$ pyrochlores.[25]

As mentioned above, bulk BZN has been studied for a variety of applications due to its relatively low firing temperature, high permittivity, high Q and small TCC.[5] It has been reported that bulk BZN has a low sintering temperature, below 950 °C. $Bi_{1.5}Zn_{1.0}Nb_{1.5}O_7$ has a permittivity of 150, TCC of -400 ppm/°C, while $Bi_2Zn_{2/3}Nb_{4/3}O_7$ has a permittivity of 80 and TCC of 200 ppm/°C.[7]

Using the Materials Research Laboratory's facilities, ZnO was not detected in bulk $Bi_{1.5}Zn_{1.0}Nb_{1.5}O_7$.[29] However, it was found that bulk $Bi_{1.5}Zn_{1.0}Nb_{1.5}O_7$ showed XRD peaks corresponding to ZnO (Figure 1-3) when measured at NIST's (National Institute of Standards and Technology) facilities, which have better signal to noise ratios.[29] Calculated from the relative peak intensities, the XRD patterns showed 50 mol% excess ZnO. It was found that a BZN composition can be synthesized in bulk ceramics that does not contain any ZnO second phase: $Bi_{1.5}Zn_{0.92}Nb_{1.5}O_{6.92}$.[29] The amount of Zn could not be reduced below 0.84 without resulting in appearance of $BiNbO_4$.[29]

Bulk bismuth-based pyrochlore systems show a low temperature dielectric relaxation.[5,17-20,28,29] This behavior has been reported for bulk $Bi_{1.5}Zn_{1.0}Nb_{1.5}O_7$.[3,5,29]

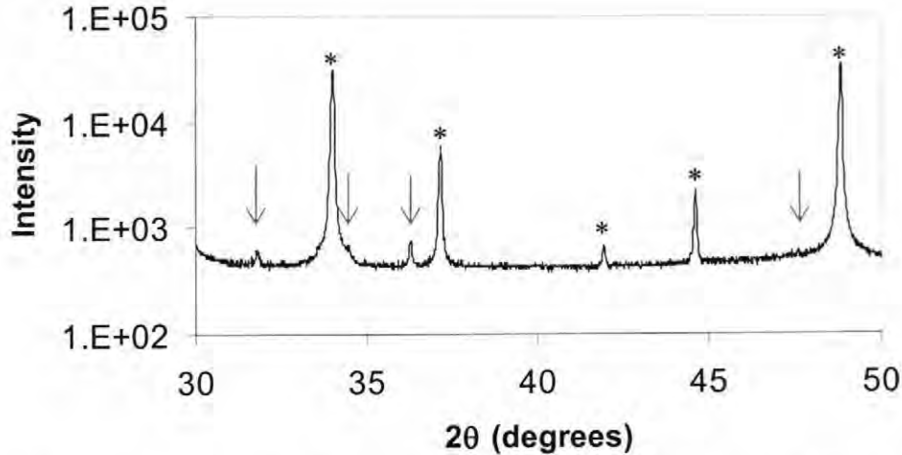

Figure 1-3: XRD pattern of bulk $Bi_{1.5}Zn_{1.0}Nb_{1.5}O_7$, with BZN peaks indicated by * and arrows indicating positions of ZnO peaks. (Courtesy of Dr. Igor Levin, NIST)

Kamba et al. studied this dielectric relaxation in $Bi_{1.5}Zn_{1.0}Nb_{1.5}O_7$ over the temperature range 10 K – 400 K, and the frequency range 100 Hz and 100 THz.[30] This large temperature and frequency range improves the accuracy of the resulting analysis over measurements made within a smaller range. The large frequency range was accomplished by using low-frequency capacitance bridges (100 Hz – 1 MHz), a high-frequency coaxial technique (1 MHz – 1.8 GHz) , time domain transmission THz spectroscopy (90 – 900 GHz), and infrared spectroscopy (0.6 – 100 THz).[30] From the dielectric dispersion data, the distribution function of the relaxation frequencies, T(Ω), were modeled.[30] Over this temperature range, the low frequency edges of T(Ω) were well fit by the Arrhenius law,

$$\frac{1}{\tau_c} = \upsilon_o \exp\left[-\frac{E_a}{k_B T}\right] \tag{1.1}$$

where τ_c is the characteristic relaxation time, υ_o is attempt jump frequency, E_a is the activation energy, and k_B is Boltzmann constant, with $\upsilon_o = 6.13*10^{12}$ Hz and $E_a = 0.202$ eV.[30] Their data for low frequency edges of T(Ω) were also fit to the Vogel-Fulcher law,

$$\frac{1}{\tau_c} = \upsilon_0 \exp\left[-\frac{E_a}{k_B(T - T_f)}\right] \qquad (1.2)$$

where T_f is the freezing temperature, which is defined as the temperature where the dynamic reorientation of dipolar cluster polarization can no longer be thermally activated. T_f was calculated to be only 0.4 K; since this is nearly 0, there is little difference between the two models.[30] Nino et al. fit the maximum in loss tangent to the Arrhenius law over the frequency range of 1 kHz to 1 GHz and found $\upsilon_o = 1.50*10^{13}$ Hz and $E_a = 0.156$ eV.[5]

Kamba et al. attributed the relaxation in $Bi_{1.5}Zn_{1.0}Nb_{1.5}O_7$ to the broad distribution of relaxation times resulting from the mixture of Bi and Zn atoms or vacancies on the A positions.[30] Random fields are caused by electronic instabilities[31] (such as the disorder on the A site in pyrochlores), and their contribution to the relaxation in other systems will be discussed in Section 1.5.3. The description of this relaxation by Kamba et al. is reinforced by the observation that $Bi_2Zn_{2/3}Nb_{4/3}O_7$ is completely ordered on the A site, and does not show any relaxation behavior.[30] Also, $Bi_{1.5}Zn_{1.0}Ta_{1.5}O_7$, which likely also has mixed occupancy on the A site of Bi and Zn, shows a dielectric relaxation.[32]

1.2 BZN Thin Films

In addition to bulk BZN, thin films of BZN have been studied by Ren et al.[15] Unlike most ferroelectric thin films, it was found that the dielectric properties of BZN

thin films are comparable to those reported for bulk BZN.[15] When fired at 750 °C, $Bi_{1.5}Zn_{1.0}Nb_{1.5}O_7$ thin films have a permittivity of 150, loss tangent < 0.005, and temperature coefficient of capacitance (TCC) of -400 ppm/°C, all of which are comparable to reported values for bulk BZN ceramics.[5,7] Similarly, for $Bi_2Zn_{2/3}Nb_{4/3}O_7$, its permittivity of 80, loss tangent < 0.005, and TCC of 150 ppm/°C were comparable to bulk values.[5,7] The similarity between the values for bulk and thin film BZN contrasts to that normally observed in ferroelectrics such as $Ba_{0.7}Sr_{0.3}TiO_3$ (BST), in which thin films tend to have lower permittivities than bulk specimens.[33,34]

When metallorganic deposited (MOD) $Bi_{1.5}Zn_{1.0}Nb_{1.5}O_7$ thin films are fired between 550 °C and 750 °C , they crystallize into the cubic pyrochlore structure (Figure 1-4a).[15] $Bi_2Zn_{2/3}Nb_{4/3}O_7$ crystallizes into the cubic pyrochlore structure at 550-650 °C, into the monoclinic zirconolite structure at 750 °C, and shows a mixture of the two phases at temperatures between 650 - 750 °C (Figure 1-4b).[15] At firing temperatures below 550 °C, both compositions were found to be amorphous.[15] However, dielectric properties of these amorphous films were not reported. Also, it was not reported whether or not annealing amorphous films at their firing temperature for significantly longer times resulted in crystalline films.

$Bi_{1.5}Zn_{1.0}Nb_{1.5}O_7$ thin films have been found to have an electric field-tunable permittivity, making them potentially useful for some microwave applications (Figure 1-5a). Thin film ferroelectric oxides, such as BST, have been investigated recently for use as electric field tunable microwave applications, such as field-dependent capacitors, tunable resonators, phase shifters, frequency-agile filters, variable-power dividers, and

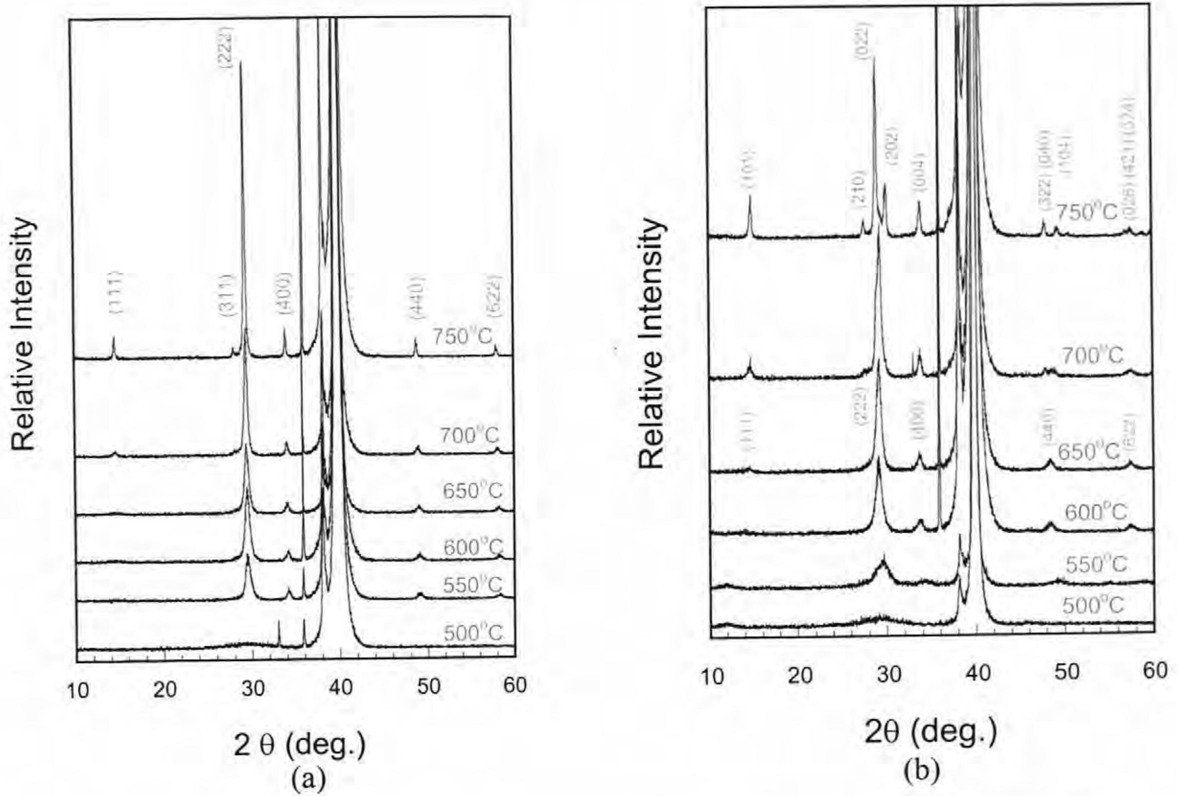

Figure 1-4: X-Ray Diffraction (XRD) patterns showing structure of BZN thin films as a function of firing temperature. (a) $Bi_{1.5}Zn_{1.0}Nb_{1.5}O_7$, (b) $Bi_2Zn_{2/3}Nb_{4/3}O_7$.[15]

variable frequency oscillators.[1] This variable permittivity gives rise to the tunability which is defined:

$$\text{tunability (\%)} = \frac{(C_{max} - C_{min})}{C_{min}} \text{ x } 100 \qquad (1.3)$$

where C_{max} and C_{min} are the maximum and minimum capacitance values measured. This tunability arises from the non-linear nature of the polarizability.[1] Over the dc electric field range reported by Ren et al.,[15] –830 kV/cm to 830 kV/cm, $Bi_2Zn_{2/3}Nb_{4/3}O_7$ was not found to have a tunable permittivity (Figure 1-5b).

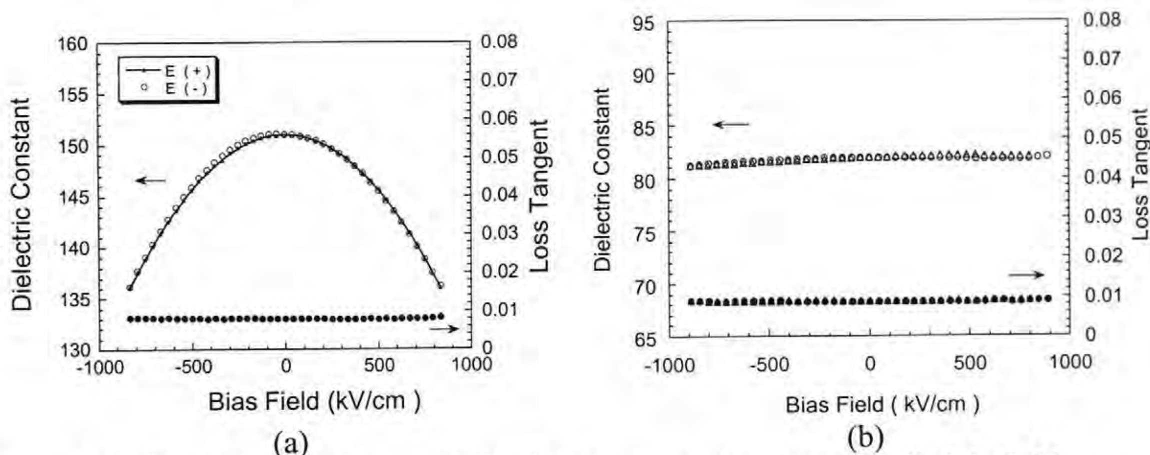

Figure 1-5: Permittivity and loss of BZN thin films as a function of applied dc field. (a) $Bi_{1.5}Zn_{1.0}Nb_{1.5}O_7$, (b) $Bi_2Zn_{2/3}Nb_{4/3}O_7$.[15]

$Bi_{1.5}Zn_{1.0}Nb_{1.5}O_7$ thin films show a low temperature relaxation in the permittivity (Figure 1-6). This relaxation was accompanied by a peak in the loss tangent as a function of frequency and temperature. It was suggested that $Bi_{1.5}Zn_{1.0}Nb_{1.5}O_7$ fit an Arrhenius equation (Equation 1.1) as opposed to a Vogel-Fulcher relation (Equation 1.2), with $\upsilon_o = 2*10^{13}$ Hz and $E_a = 0.13$ eV.[15] Both values are similar to those found for bulk $Bi_{1.5}Zn_{1.0}Nb_{1.5}O_7$ (Section 1.1), and υ_o is on the order of ionic lattice vibrations.[15]

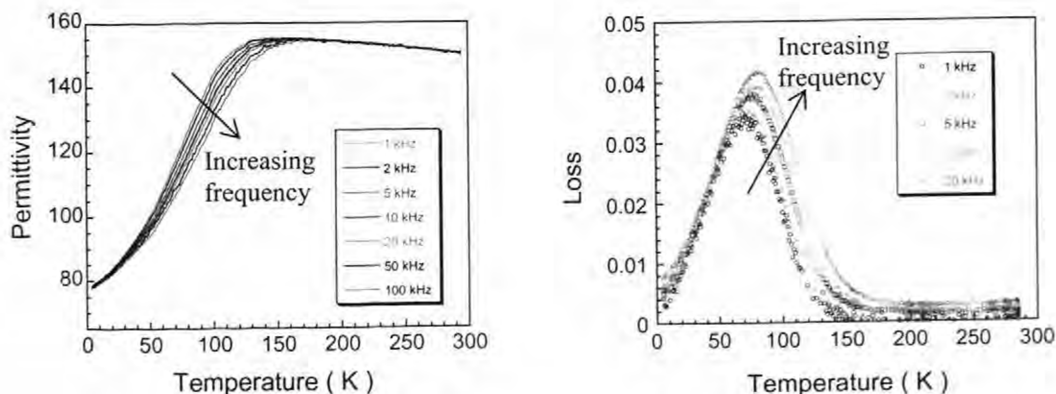

Figure 1-6: Measuring temperature dependence of permittivity and loss tangent of $Bi_{1.5}Zn_{1.0}Nb_{1.5}O_7$ films fired at 750 °C.[15]

Cheng et al. studied $Bi_2Zn_{2/3}Nb_{4/3}O_7$ thin films deposited by pulsed laser deposition (PLD).[35] They found that $Bi_2Zn_{2/3}Nb_{4/3}O_7$ crystallized when deposited onto indium-tin oxide substrates at temperatures in the range 475 – 525 °C. The maximum permittivity was approximately 300, and no Q values were reported. A possible source of inflated permittivity measurements is space charge accumulation. In another study Chen et al. measured the permittivity of $Bi_2Zn_{2/3}Nb_{4/3}O_7$ thin films in the THz regime using a THz-TDS (time domain spectroscopic) technique.[36] Their results showed a permittivity of 32 in the THz regime, which is lower than samples of the same composition measured at the same frequency by Kamba et al.[29] In a study by Cheng et al.,[37] $Bi_2Zn_{2/3}Nb_{4/3}O_7$ films were also deposited using PLD, although their target had a permittivity of only 67, which is much lower than the permittivity Nino et al.[5] reports for the same composition. This lower permittivity of the target could be due to the processing conditions not being optimized. The permittivity of thin films were also estimated using Fourier transform infrared (FTIR) spectroscopy,[38] and again the permittivity was lower than reported by Nino for bulk samples of the same composition.[29] The permittivity of $Bi_2Zn_{2/3}Nb_{4/3}O_7$ was also measured using optical transmission spectroscopy,[36] resulting in a permittivity of 4.75, which would correspond to electronic polarizability.

1.3 Dipole Glasses

Since BZN shows some properties similar to dipole glasses, such as a dielectric relaxation, some properties of dipole glasses will be summarized. Dipole glasses are similar to spin glasses that are found in magnetic systems. Glassy materials have at least

two characteristics: randomness caused by disorder (usually accompanied by clustering), and freezing that results from a transition into a frustrated state.[39] The disorder can be caused by structural or chemical factors, and leads to the local symmetry being lower than the global symmetry.[39]

Dipole glasses show a peak in the permittivity when measured as a function of temperature, which broadens with increasing temperature. In addition, dipole glasses have a relaxation of the permittivity, with the maximum in the permittivity peak shifting to higher temperatures with increasing frequency. This peak in permittivity shows a Vogel-Fulcher dependence (Equation 1.2).[39] However, the temperature at which the permittivity maximum occurs tends to show less of a shift at lower frequencies, and reaches a constant value, which is referred to as a freezing temperature.[39]

1.4 Ferroelectric Relaxors

Since cubic BZN exhibits a relaxation of the permittivity, it is useful to contrast its behavior with that of ferroelectric relaxors. Relaxors are ferroelectric systems which cannot establish long range polar ordering due to an inhomogeneity.[39] Relaxor ferroelectrics can be summarized by four characteristics: (1) a peak in the low frequency susceptibility which broadens with increasing frequency, (2) a relaxation of the permittivity over a wide frequency range, (3) strong deviation from Curie-Weiss behavior, and (4) the existence of remanence below a characteristic temperature.[39]

In relaxors, the local symmetry is lower than the global, but the long-range polar ordering typical of a ferroelectric state cannot form. Relaxor behavior results from this

broken symmetry. A global phase transition is prevented, although local transitions can occur. Burns et al. showed that local polarization exists in relaxors until temperatures far above the permittivity maximum.[40] They calculated the local polarization from the temperature dependence of the refractive indices using a phenomenological model. Based on these results, Burns proposed a glassy polarization mechanism that was on the scale of several unit cells and analogous to spin glasses.[41] Randall et al. showed that the development of long range order occurred by coarsening of B-site cation-ordered regions.[42] This work suggests that the relaxor behavior depends on the degree of long range order. Stronger correlations can develop with increasing long range order, and the relaxor behavior is thereby decreased. Correlations can be minimized by introducing an inhomogeneity that breaks the local translational symmetry of the polarization, which can effectively diffuse the dielectric response.

1.5 Models of Relaxor Ferroelectrics

1.5.1 Superparaelectric Model

Cross proposed the superparaelectric model to describe relaxor ferroelectrics, which is analogous to superparamagnetism.[43] In this model, dipoles form non-interacting polar regions, or clusters. Each cluster shows ferroelectric behavior, with several equivalent polarization orientations possible. Changing of the polarization direction is a thermally activated process. The experimentally observed increase in permittivity of $Pb(Mg_{1/3}Nb_{2/3})O_3$ (PMN) upon cooling can be explained using this model since there is a decrease in randomness resulting from thermal agitation.

The dielectric dispersion is attributed to the size distribution of the clusters. The relaxation time, τ, of a cluster increases upon cooling, and at some temperature a frequency is reached at which the region does not respond to the applied field, or is blocked. A distribution of sizes of the polar regions in a material results in a distribution of relaxation times. This leads to a distribution of temperatures at which polar regions become blocked, which leads to the observed frequency-dependent peak in the permittivity as a function of temperature.

Bell calculated the dielectric properties of relaxors using this superparaelectric model, and found that relaxor behavior can indeed be described by gradual blocking of thermally activated changes in polarization directions within isolated polar regions.[44,45] He used Landau-Ginsburg-Devonshire (LGD) phenomenological theory of ferroelectrics to describe the behavior of the clusters. It was assumed that there was a distribution of volumes of the regions, and these volumes were temperature-dependent. Incorporating the assumption that individual regions have a single phase transition, the calculations showed good agreement with observed results. Bell also found that, with some exceptions, this model gave a good qualitative and quantitative fit to measured temperature- and frequency-dependent behavior of the permittivity of PMN.[45]

1.5.2 Glassy Model

Relaxors have also been proposed to be glassy-like materials[46-48] with similar behavior as other glassy systems, such as magnetic spin glasses[41] and dielectric dipole glasses.[49] The dipole glass model of relaxors is considered an extension of the

superparaelectric model. The difference between the dipole glass and the superparaelectric models is that in the former, the superparaelectric clusters interact, while in the latter the clusters are isolated. The glassy behavior arises from increased interactions upon cooling. When cooled to a temperature, T_g, disordered polar regions freeze into a metastable frozen state with random orientations of the polarization. This freezing is a cooperative phenomenon, since it results from interactions between the polar clusters, and is similar to a phase transition. The experimental evidence that supports the glassy nature of relaxors are:[46,50-52] (1) the linear permittivity shows a frequency-dependent maximum as a function of temperature, with this maximum showing a Vogel-Fulcher dependence (Equation 1.2), (2) a broad relaxation time spectrum, (3) lack of long range order, especially at lower temperatures, (4) the appearance of non-ergodic behavior, with an onset temperature approaching T_f obtained from fitting the temperature-dependence of τ to the Vogel-Fulcher law, and (5) the non-linear components of dielectric response as a function of temperature show peaks that are not related to the field-induced phase transition into a macroscopic ferroelectric state.[45]

When contrasting the superparaelectric and glassy models, point (5) is important.[45] Freezing in a glass is similar to a phase transition with a definite transition temperature, T_g. For spin glasses, non-linear terms in the series expansion of polarization as a function of electric field should show critical behavior near T_g, but the linear term should not show critical behavior at T_g. However, in the superparaelectric model, freezing is a gradual process with no definite transition temperature, so there should not be any critical behavior.[45]

Some experimental data reported for PMN that have not been explained by the glassy model of relaxors are the absence of long range order at low temperatures and the increase in distribution of relaxation times as the temperature approaches T_f.[53,54] Also, it has been shown that nonergodic behavior at temperatures below T_f is not exclusive of a glassy material, since this behavior is also found in a system in which local random fields prevent a structural phase transition into the ferroelectric state.[53]

1.5.3 Models Incorporating Random Fields

Kleeman et al.[53,54] incorporated the effects of random fields into the dipole glass model to describe the data in the preceding paragraph, and suggested that at low temperatures a phase transition occurs in PMN from disordered polar regions into a ferroelectric state with small frozen domains. Other experimental evidence that support this model include:[53] (1) Barkhausen jumps occur at low temperatures, which are caused by sudden domain rearrangements, (2) the permittivity decreases when an external dc field is applied, explained through a macroscopic ferroelectric state which occurs when the applied field overrides the disordering random fields, and (3) the transition into a ferroelectric state can be determined from the temperature dependence of the remanent polarization.

Kleeman et al.[53,54] attributed the source of these random fields to the crystalline disorder typically found in relaxors. Some possible sources of random fields[45] in Pb-based perovskites are equivalent lattice sites that are occupied by different ions which

usually have different valencies[55,56] (for PMN: Mg^{2+} and Nb^{5+}), and lattice defects, for example resulting from vacancies on the Pb^{2+} sites.[57]

The effects of random fields have also been incorporated into the superparaelectric model.[58] In the superparaelectric model, an energy barrier separates the different orientations of the polarization. The distribution of relaxation times is attributed to a distribution of heights of this energy barrier. However if random fields are taken into consideration, they will produce a distorted potential barrier, leading to a difference in equilibrium polarization directions.

Vugmeister[59] proposed a phenomenological model of relaxors which incorporates random fields. According to Vugmeister, this model can be used to analyze a variety of properties of relaxors and other random dielectric systems. For example, it has been used to describe pure relaxor behavior in PMN and the simultaneous presence of relaxor behavior mixed with a phase transition into a ferroelectric state in $Pb(Sc_{0.5}Ta_{0.5})O_3$, or PST.[60] Vugmeister's model showed good agreement with the experimentally determined temperature and frequency dependence of the real part of the permittivity for both PST and PMN. However, a limitation of this model is found when comparing calculated and experimental data for the imaginary part of the permittivity, since the calculations did not compare well with the experimentally observed behavior.[45]

Another drawback to this model was reported by Chu et al.[60] They experimentally found that the freezing temperature in the Vogel-Fulcher law occurred at a similar temperature as the T_c of PST, which is the temperature at which the phase transition from the disordered state to the ferroelectric state occurred. This suggests that

both the distribution of relaxation times and the phase transition were linked. However, in Vugmeister's model the dynamic and thermodynamic properties are not related since the former was determined from the temperature dependence of the relaxation times, while the latter were determined by the temperature dependence of coefficients of the series expansion of the polarization.[45]

A random-field Potts model was proposed by Qian and Bursill.[61,62] They examined the temperature and frequency dependence of the linear permittivity for both PMN and PST. For both materials, the modeled behavior agreed with the experimental behavior.[60]

In summary, there is considerable disagreement over which of the models of relaxors described above is accurate. One of the main reasons for this is the same experimental data are used for all models. Also, the models use the same physical model of PMN (randomly distributed polar regions in non-polar surroundings) to describe the frequency dispersion and distribution of relaxation times of the linear permittivity. In contrast, a breathing model[45,63] has been proposed that is based on a different microscopic picture of PMN than the ones described thus far.

1.5.4 Breathing Model

A model that has been proposed by Glazounov and Tagantsev to describe relaxor ferroelectrics is the breathing model.[45,63] This model is fundamentally different from the ones described above. In this model the ergodic phase of PMN is modeled as polar regions surrounded by a non-polar phase. What differs from the above models in the case

of the breathing model is that the polarization in each polar region does not change orientation due to thermal agitation; instead its orientation is along one of the eight <111> directions dictated by rhombehedral symmetry. The interphase boundaries between the polar and nonpolar phases are determined by the distribution of pinning centers. Following interface roughening arguments,[64] these boundaries are not straight; they will become 'rough' with a length L_c. When an external dc field is applied, pressure is exerted on the interphase boundary. This pressure will lead to a section of length L_c which moves, thereby affecting the volume of the polar region, and also its dipole moment.

One of the advantages of the breathing model over the ones described above is that it can be used to describe the behavior of PMN under applied ac and dc fields. At low ac fields, the permittivity of PMN increases, while under dc fields, the permittivity decreases. In the temperature and frequency range that the dispersion of the permittivity of PMN occurs, Glazounov and Tagantsev describe the effects of dc and ac fields on the length, L_c, of the moving section of the boundary as follows: under either an ac or dc bias, L_c is both temperature- and frequency-dependent. Decreasing temperature and increasing frequency will decrease L_c. The frequency dependence results from depinning of the interphase boundary. Decreasing the magnitude of the ac field will also decrease L_c. The dispersion in permittivity results from a distribution of magnitudes of L_c that results in a distribution of dipole moments.

1.6 Thesis Objectives

The three main areas of focus for this thesis were synthesizing and characterizing a new cubic BZN composition, determining the ac and dc field tunability of permittivity, and measuring the leakage characteristics of BZN films. As described in Section 1.1, the effect of Zn occupancy on the A-site of bulk BZN was studied by Nino.[29] However, single-phase bulk samples with Zn content less than 0.84 could not be prepared. One of the goals of this thesis was to prepare and characterize MOD-processed BZN films with the composition $Bi_{1.5}Zn_{0.5}Nb_{1.5}O_{6.5}$, which has not been previously studied.

The function of some filters would be improved by the use of tunable dielectrics. If BZN films are to be used in applications such as these, the tunability of the permittivity under high fields must be better understood. Also, by analyzing tunability, insight can be gained into the behavior of the polarization as a function of field. A second goal of this thesis was to explore the tunability of BZN films under both ac fields and dc fields. The high dc field results were used to describe the non-linear polarizability, while the variation of permittivity with ac field was explored for BZN films. The possible mechanisms responsible for the dielectric relaxation in BZN films can be narrowed using these results.

In addition, if BZN films are to be used in applications such as decoupling capacitors in integrated circuits, the leakage behavior of the films must be characterized. The variation of leakage with dc field was studied, as well as the role of different top electrode metals.

1.7 References

1. J.J. Giumarra, "The Effects of Annealing on the Dielectric Response of Barium Strontium Titanate Thin Films," M.S. Thesis, University of Illinois, Chicago, 2000.

2. C.-L. Huang and M.-H. Weng, "Low-Fire $BiTaO_4$ Dielectric Ceramics for Microwave Applications," *Mater. Lett.* **43** (1-2) 32-5 (2000).

3. D. Cann, C.A. Randall and T.R. Shrout, "Investigation of the Dielectric Properties of Bismuth Pyrochlores," *Solid State Commun.* **100** (7) 529-34 (1996).

4. J.C. Nino, M.T. Lanagan and C.A. Randall, "Phase Formation and Reactions in the Bi_2O_3-ZnO-Nb_2O_5 – Ag Pyrochlore System," *J. Mater. Res.* **16** (5) 1460-4 (2001).

5. J.C. Nino, M.T. Lanagan and C.A. Randall, "Dielectric Relaxation in the Bi_2O_3-ZnO-Nb_2O_5 Cubic Pyrochlore," *J. Appl. Phys.* **89** (8) 4512-5 (2001).

6. M.F. Yan, H.C. Ling and W.W. Rhoads, "Low-Firing, Temperature-Stable Dielectric Compositions Based on Bismuth Nickel Zinc Niobates," *J. Am. Ceram. Soc.* **73** 1106-7 (1990).

7. D. Liu, Y. Liu, S. Huang and X. Yao, "Phase Structure and Dielectric Properties of Bi_2O_3-ZnO-Nb_2O_5-Based Dielectric Ceramics," *J. Am. Ceram. Soc.* **76** (8) 2129-32 (1993).

8. X. Wang, H. Wang and X. Yao, "Structures, Phase Transformations, and Dielectric Properties of Pyrochlores Containing Bismuth," *J. Am. Ceram. Soc.* **80** (10) 2745-8 (1997).

9. H. Wang and X. Yao, "Structure and Dielectric Properties of Pyrochlore-Fluorite Biphase Ceramics in the Bi_2O_3-ZnO-Nb_2O_5 System," *J. Mater. Res.* **16** (1) 83-7 (2001).

10. L.D. Smith, R.E. Anderson, D.W. Forehand, T.J. Pelc and T. Roy, "Power Distribution System Design Methodology and Capacitor Selection for Modern CMOS Technology," *IEEE Trans. on Adv. Packag.* **22** (3) 284-91 (1999).

11. H.-T.D. Chen, "Ferroelectric Thin and Thick Films for Sensing and Decoupling Functions," Ph.D. Thesis, Pennsylvania State University, 1996.

12. E.E. Davidson, "Electrical Design of a High Speed Computer Package," *IBM J. Res. Develop.* **26** (3) 349-60 (1982).

13. P. Gallotello, "Testing a High-Rel Decoupling Capacitor Socket," *Connection Technology* **6** (4) 39-40 (1990).

14. G.A. Katopis, "Delta-I Noise Specification for a High-Performance Computing Machine," *Proc. IEEE* **73** (9) 1405-15 (1985).

15. W. Ren, S. Trolier-McKinstry, C.A. Randall and T.R. Shrout, "Bismuth Zinc Niobate Pyrochlore Dielectric Thin Films for Capacitive Applications," *J. Appl. Phys.* **89** (1) 767-74 (2001).

16. J.Z. Wei, L.Y. Zhang and X. Yao, "Melting Properties of Bi_2O_3-ZnO-Nb_2O_5-Based Dielectric Ceramics," *J. Am. Ceram. Soc.* **82** (9) 2551-2 (1999).

17. J.C. Nino, T. Sogabe, M.T. Lanagan, T.R. Shrout and C.A. Randall, "NPO Capacitors Based on Bi-Pyrochlore Dielectric Materials," *Extended Abstract 9th US-Japan Seminar on Dielectric and Piezoelectric Ceramics* (Okinawa, 1999) 453-7.

18. G.I. Golovshchikova, V.A. Isupov, A.G. Tutov, I.E. Myl'nikova, P.A. Nikitina and O.I. Tulinova, "Relaxational Character of the Dielectric Polarization in the Region of the Phase Change of New Compounds of the Pyrochlore Type," *Sov. Phys.-Solid State* **14** 2539-42 (1973).

19. G.A. Smolenskii, V.A. Isupov, G.I. Golovshchikova and A.G. Tutov, "New Compounds with the Pyrochlore Structure, and their Dielectric Properties," *Izv. Akad. Nauk SSSR Neorg. Mater.* **12** 297-301 (1976).

20. D. Bernard, J. Pannetier and J. Lucas, "Ferroelectric and Antiferroelectric Materials with Pyrochlore Structure," *Ferroelectrics* **21** 429-31 (1978).

21. H. Kagata, T. Inoue, J. Kato and I. Kameyama, "Low-Fire Bismuth-Based Dielectric Ceramics for Microwave Use," *Jpn. J. Appl. Phys.* **31** 3152-5 (1992).

22. J. Champarnaud-Mesjard, M. Manier and B. Frit, "Bismuth(III)-and Antimony(V)-Based Ceramics with Anion-Deficient Flourite Structure," *Journal of Alloys and Compounds* **188** 174-8 (1992).

23. A. Mergen and W.E. Lee, "Crystal Chemistry, Thermal Expansion and Dielectric Properties of $(Bi_{1.5}Zn_{0.5})(Zn_{0.5}Nb_{1.5})O_7$ Pyrochlore," *Mater. Res. Bull.* **32** (2) 175-89 (1997).

24. M. Valant and P. Davies, "Crystal Chemistry and Dielectric Properties of Chemically Substituted $(Bi_{1.5}Zn_{1.0}Nb_{1.5})O_7$ and $Bi_2(Zn_{2/3}Nb_{4/3})O_7$ Pyrochlores," *J. Am. Ceram. Soc.* **83** (1) 147-53 (2000).

25. M.A. Subramanian, G. Aravamudan and G.V. Subba Rao, "Oxide Pyrochlores – A Review," *Prog. Solid State Chemistry* **15** 55-143 (1983).

26. Y. Hu and C.L. Huang, "Structure and Dielectric Properties of Bismuth-Based Dielectric Ceramics," *Mater. Chem. Phys.* **72** (1) 60-5 (2001).

27. I. Levin, T.G. Amos, J.C. Nino, T.A. Venderah, I.M. Reaney, C.A. Randall and M.T. Lanagan, "Crystal Structure of the Compound $Bi_2Zn_{2/3}Nb_{4/3}O_7$," *Mat. Res. Bull.* **17** (6) 1406-11 (2002).

28. E. Aleshin and R. Roy, "Crystal Chemistry of Pyrochlore," *J. Am. Ceram. Soc.* **45** (1) 18-25 (1962).

29. J.C. Nino, "Fundamental Structure-Property Relationships Towards Engineering of an Integrated NPO Capacitor for Bismuth Pyrochlore Systems," Ph.D. Thesis, The Pennsylvania State University, 2002.

30. S. Kamba, V. Porokhonsky, A. Pashkin, V. Bovtun, J. Petzelt, J.C. Nino, S. Trolier-McKinstry, M.T. Lanagan and C.A. Randall, "Anomalous Broad Dielectric Relaxation in $Bi_{1.5}Zn_{1.0}Nb_{1.5}O_7$ Pyrochlore," *Phys. Rev. B.* **66** (5) 054106/1-8 (2002).

31. Y. Imry and S.-K. Ma, "Random-Field Instability of the Ordered State of Continuous Symmetry," *Phys. Rev. Lett.* **35** (21) 1399-401 (1975).

32. H.-J. Youn, T. Sogabe, C.A. Randall, T.R. Shrout and M.T. Lanagan, "Phase Relations and Dielectric Properties in the Bi_2O_3-ZnO-Ta_2O_5 System," *J. Am. Ceram. Soc.* **84** (11) 2557-62 (2001).

33. R. Waser, "Dielectric Analysis of Integrated Ceramic Thin Film Capacitors," *Integr. Ferroelectr.* **15** 39-51 (1997), and references cited therein.

34. C. Basceri, S.K. Streiffer, A.I. Kingon and R. Waser, "The Dielectric Response as a Function of Temperature and Film Thickness of Fiber-Textured (Ba,Sr)TiO_3 Thin Films Grown by Chemical Vapor Deposition," *J. Appl. Phys.* **82** (5) 2497-504 (1997).

35. H.-F. Cheng, Y.-C. Cheng and I.-N. Lin, "Frequency Response of Microwave Dielectric $Bi_2(Zn_{1/3}Nb_{2/3})_2O_7$ Thin Films Laser Deposited on Indium-Tin Oxide Coated Glass," *J. Appl. Phys.* **87** (1) 479-83 (2000).

36. Y.-C. Chen, H.-F. Cheng, Y.-M. Tsau, P. Kuzel, J. Petzelt and I.-N. Lin, "Synthesis and Properties of Dielectric $Bi_2(Zn_{1/3}Nb_{2/3})_2O_7$ Thin Films," *J. Eur. Ceram. Soc.* **21** 2731-4 (2001).

37. H.-F. Cheng, Y.-C. Chen, Y.-M. Tsau, P. Kuzel, J. Petzelt, Y.-H. Zhu and I.-N. Lin, "Dielectric Properties of $Bi_2(Zn_{1/3}Nb_{2/3})_2O_7$ Electroceramics and Thin Films," *J. Eur. Ceram. Soc.* **21** 1605-8 (2001).

38. Y.-C. Chen, H.-L. Liu, H.-F. Cheng and I.-N. Lin, "Dielectric Properties of $Bi_2(Zn_{1/3}Nb_{2/3})_2O_7$ Thin Films Measured by Fourier Transform Infrared Spectroscopy," *J. Eur. Ceram. Soc.* **21** 1711-4 (2001).

39. D. Viehland, "The Glassy Behavior of Relaxor Ferroelectrics," Ph.D. Thesis, The Pennsylvania State University, 1991.

40. G. Burns and F. Dacol, "Glassy Polarization Behavior in Ferroelectric Compounds $Pb(Mg_{1/3}Nb_{2/3})O_3$ and $Pb(Zn_{1/3}Nb_{2/3})O_3$," *Sol. State Commun.* **48** (10) 853-6 (1983).

41. K. Binder and A. Young, "Spin Glasses: Experimental Facts, Theoretical Concepts, and Open Questions," *Rev. Mod. Phys.* **58** (4) 801-976 (1986).

42. C.A. Randall, D. Barber, R. Whatmore and P. Groves, "A TEM Study of Ordering in the Perovskite, $Pb(Sc_{1/2}Ta_{1/2})O_3$," *J. Mat. Sci.* **21** (12) 4456-62 (1986).

43. L.E. Cross, "Relaxor Ferroelectrics," *Ferroelectrics* **76** (3-4) 241-67 (1987).

44. A.J. Bell, "Calculations of Dielectric Properties from the Superparaelectric Model of Relaxors," *J. Phys: Condens. Matter* **5** (46) 8773-92 (1993).

45. A. Glazounov, "Non-Linear Dielectric Response of $Pb(Mg_{1/3}Nb_{2/3})O_3$ Relaxor Ferroelectric," Ph.D. Thesis, Swiss Federal Institute of Technology - Ecole Polytechnique Federale de Lausanne (EPFL), 1997.

46. D. Viehland, S.J. Jang, L.E. Cross and M. Wuttig, "Freezing of the Polarization Fluctuations in Lead Magnesium Niobate Relaxors," *J. Appl. Phys.* **68** (6) 2916-21 (1990).

47. S.B. Vakhrushev, B.E. Kvyatkovsky, A.A. Naberezhnov, N.M. Okuneva and B.P. Toperverg, "Glassy Phenomena in Disordered Perovskite-like Crystals," *Ferroelectrics* **90** 173-6 (1989).

48. N.K. Yushin, S.N. Dorogovstev and S.I. Smirnov, "Manifestation of Nonergodicity in a Ferroelectric with a Diffuse Phase Transition," *Soviet Techn. Phys. Lett.* **14** (1) 55-6 (1988).

49. U.T. Hochli, K. Knorr and A. Loidl, "Orientational Glasses," *Adv. Phys.* **39** (5) 405-614 (1990).

50. S.N. Dorogovstev and N.K. Yushin, "Acoustical Properties of Disordered Ferroelectrics," *Ferroelectrics* **112** 27-44 (1990).

51. E.V. Colla, E.Y. Koroleva, N.M. Okuneva and S.B. Vakhrushev, "Long-Term Relaxation of the Dielectric Response in Lead Magnoniobate," *Phys. Rev. Lett.* **74** (9) 1681-4 (1995).

52. N.K. Yushin and S.N. Dorogovstev, "Acoustic and Dielectric Relaxation in Ferroelectrics with Diffuse Phase Transition," *Ferroelectrics* **143** 49-57 (1993).

53. V. Westphal, W. Kleemann and M.D. Glinchuk, "Diffuse Phase Transition and Random-Field-Induced Domain States of the 'Relaxor' Ferroelectric $PbMg_{1/3}Nb_{2/3}O_3$," *Phys. Rev. Lett.* **68** (6) 847-50 (1992).

54. W. Kleemann, "Random-Field-Induced Antiferromagnetic, Ferroelectric and Structural Domain States," *Int. J. Mod. Phys. B* **7** (13) 2469-507 (1993).

55. G.A. Smolenskii, "Physical Phenomena in Ferroelectrics with Diffused Phase Transition," *J. Phys. Soc. Jpn* **28 suppl**. 26-37 (1970).

56. V.A. Isupov, "Causes of Phase-Transition Broadening and the Nature of Dielectric Polarization Relaxation in Some Ferroelectrics," *Sov. Phys. Solid State* **5** (1) 136-40 (1963).

57. F. Chu, I.M. Reaney and N. Setter, "Role of Defects in the Ferroelectric Relaxor Lead Scandium Tantalate," *J. Am. Ceram. Soc.* **78** (7) 1947-52 (1995).

58. K.S. Gilroy and W.A. Phillips, "An Asymmetric Double-Well Potential Model for Structural Relaxation Processes in Amorphous Materials," *Phil. Mag. B* **43** (5) 735-46 (1981).

59. B.E. Vugmeister and H. Rabitz, "A Phenomenology of Relaxor Ferroelectrics," *Ferroelectrics* **201** (1-4) 33-42 (1997).

60. F. Chu, N. Setter and A.K. Tagantsev, "The Spontaneous Relaxor-Ferroelectric Transition of $Pb(Sc_{0.5}Ta_{0.5})O_3$," *J. Appl. Phys.* **74** (8) 5129-34 (1993).

61. H. Qian and L.A. Bursill, "Phenomenological Theory of the Dielectric Response of Lead Magnesium Niobate and Lead Scandium Tantalate," *Int. J. Mod. Phys. B* **10** (16) 2007-25 (1996).

62. H. Qian and L.A. Bursill, "Random-Field Potts Model for the Polar Domains of Lead Magnesium Niobate and Lead Scandium Tantalate," *Int. J. Mod. Phys. B* **10** (16) 2027-47 (1996).

63. A.E. Glazounov and A.K. Tagantsev, "Crossover in a Non-Analytical Behavior of Dielectric Non-Linearity in $PbMg_{1/3}Nb_{2/3}O_3$ Relaxor Ferroelectrics," *J. Phys.: Condens. Matter* **10** 8863-80 (1998).

64. T. Nattermann, Y. Shapir and I. Vilfan, "Interface Pinning and Dynamics in Random Systems," *Phys. Rev. B* **42** (13) 8577-86 (1990).

Chapter 2

EXPERIMENTAL PROCEDURE

Metallorganic deposition (MOD) was used to deposit BZN on platinized silicon wafers. This process is advantageous because it allows precise composition control, has good reproducibility, enables deposition over large area substrates, has low processing temperatures and low cost. In this section, the deposition and processing conditions are reported and the electrical characterization methods are described. Three compositions of BZN thin films were investigated in this study: $Bi_{1.5}Zn_{1.0}Nb_{1.5}O_7$, $Bi_{1.5}Zn_{0.5}Nb_{1.5}O_{6.5}$, and $Bi_2Zn_{2/3}Nb_{4/3}O_7$.

2.1 Solution Preparation

The solution was prepared in a manner similar to that previously reported for BZN films.[1] The precursors used were bismuth acetate, zinc acetate dihydrate (Aldrich Chemical Company, Inc, Milwaukee, WI) and niobium ethoxide (Chemat Technology, Inc, Northridge, CA). The solvents used were 2-methoxyethanol (2-MOE), pyridine, and glacial acetic acid (Aldrich). Zinc acetate dihydrate and 2-MOE were combined, then heated to 120 °C and vacuum distilled in a rotary evaporator in order to remove any

water. Niobium ethoxide was mixed with 2-MOE, and then added to the zinc solution and refluxed under argon at 120 °C for 1 h, then vacuum distilled to remove by-products. Bismuth was introduced into the system by first combining bismuth acetate and pyridine and stirring for 5 min. Glacial acetic acid (30 volume percent) was added and the solution was stirred for 0.5 h until the solution became clear. This bismuth solution was then added to the (Zn, Nb) solution and refluxed under argon at 120 °C for 15 min. Finally, the solution was vacuum distilled and 2-MOE was added to the final solution until a concentration of 0.3 M was obtained.

2.2 Thin Film Deposition

Thin films were deposited as previously reported for BZN films.[1] To prepare thin films, the precursor solution was spin coated at 3000 rpm for 30 s on Pt-coated Si wafers Pt(175nm)/Ti(20nm)/SiO_2(500nm)/Si (Ramtron International Corp, Colorado Springs, CO). The substrate was then placed on a hotplate at 350 °C for 1 min to remove organics from the film. This procedure was repeated to build up the film thickness, typically 0.3-0.4 μm, or 3-4 layers. A rapid thermal annealer was used to crystallize the films, with a heating rate of 100 °C/min and a soak time of 120 s in flowing air. If thinner samples were desired than obtained through the processing described above, the precursor solution was diluted to 0.15-0.25 M with 2-MOE before spin coating.

2.3 Characterization

The thermal decomposition of the $Bi_{1.5}Zn_{0.5}Nb_{1.5}O_{6.5}$ precursor solution was measured using a TA DTA1600 differential thermal analyzer at 10 °C/min (TA Instruments, Inc., New Castle, DE). To remove some of the solvent, the precursor solution was dried at 120 °C for 3 hrs before measuring, resulting in a gel-like consistency for the sample. For comparison, the thermal decomposition of $Bi_{1.5}Zn_{1.0}Nb_{1.5}O_7$ and $Bi_2Zn_{2/3}Nb_{4/3}O_7$ are reported in Ref. 1.

The films were characterized with a Scintag DMC-105 X-ray diffractometer (Scintag, Inc., Sunnyvale, CA) using CuK_{α} radiation between 10 ° and 60 ° 2θ at a scan rate of 1 °/min. In order to measure electrical properties, an array of Pt dots ranging from 0.5 mm to 1.15 mm in diameter were sputtered onto the films through a shadow mask to form the top electrodes in a Pt/BZN/Pt configuration. The films were then annealed 50-100 °C below their crystallization temperature for 45-60 s to improve the Pt-BZN interface of the top electrode. If a much lower temperature or a shorter anneal was used, the value of the loss tangent was higher, while higher temperatures and longer times did not affect the loss tangent. The areas of the top electrodes were measured using an optical microscope. To gain access to the bottom electrode, a corner of each film was etched with a 15 % HF solution until the bottom Pt layer was exposed, then rinsed with ethanol. After etching, the film thickness was measured by an Alpha-Step 500 surface profiler (Tencor, Portsmouth, NH).

Pt top electrodes were not used for the films that were prepared by diluting the 0.3 M solution described above. Because of the high incidence of electrical shorts, smaller

electrodes than could be obtained via shadow masking were required. Thus, the top electrodes for these samples were Cr/Au. The Cr and the Au were deposited using e-beam and thermal evaporation, respectively, and the electrodes were patterned using standard optical lithography techniques. The Cr layer was used as an adhesion layer for the Au. After patterning of the photoresist (1813; Shipley Co., Marlborough, MA), the Au was etched using a mixture of 45 % potassium iodide and 55 % iodine complex (Transene Inc., Danvers, MA), and the Cr was etched using a mixture of 6 % nitric acid, 16 % ceric ammonium nitrate, and 78 % H_2O (Transene), then the films were rinsed in deionized water. The electrodes were not annealed in this case since reasonable loss tangents were obtained without annealing. This is possibly due to the lower level of contamination and/or damage at the film-electrode interface using e-beam and thermal evaporation when compared with the typically-used sputtering through a shadow mask.

The low-field dielectric properties of the BZN films were measured with a Hewlett Packard 4192A LF Impedance Analyzer (Agilent Technologies, Inc., Palo Alto, CA) with an ac oscillation voltage of 0.03 V rms over the frequency range 1 kHz to 100 kHz. Temperature coefficient of capacitance measurements utilized the HP 4274A Multi-Frequency LCR Meter (Agilent). The temperature was adjusted using a Delta Design 2300 oven (Delta Design, Inc., Poway, CA). During these TCC measurements, the samples were heated to 120 °C and the capacitance and loss were measured on cooling to –50 °C. The heating step was done first to remove moisture from the chamber. The samples were measured by placing them in a sample holder that connected to the LCR meter though the oven door. The sample itself was contacted using probe tips on

the end of wires that could be bent to change the position of the probe in order to measure a number of electrodes. Also, the wires could be bent to adjust the pressure on the electrodes to ensure a good contact.

The high dc field measurements were made using the HP 4274A Multi-Frequency LCR Meter, with a Keithley Instruments 240 A high voltage supply (Keithley Instruments, Inc., Cleveland, OH). A dc voltage sweep was made starting at 0 V, increasing to the maximum positive voltage, decreasing to the maximum negative voltage, and returning to 0 V. An oscillation voltage of 0.03 V was used. These measurements were conducted at room temperature, 77 K (using liquid nitrogen), and intermediate temperatures using the Delta Design oven. The lower temperatures were used so a higher field could be applied without breakdown occurring due to a decrease in electrical conductivity.

The low temperature permittivity and loss measurements utilized the HP 4284A Precision LCR Meter (Agilent) over the frequency range 100 Hz to 100 kHz. The low temperature was reached by cooling the sample at approximately 2 °C/min in a dewar filled with liquid helium. The ac oscillation voltage of 0.03 V was used.

The effect of high ac fields on permittivity was measured using a HP 4284A Precision LCR Meter. This instrument was used for these measurements due to its ability to provide a higher ac voltage (20 V) than either the HP 4284A or the HP 4274A used above. A Delta Design 2300 oven was used to adjust the temperature.

Leakage currents were measured using a HP 4156B Precision Semiconductor Parameter Analyzer, with the electrical probes enclosed in a glovebox with a dry nitrogen

environment. The voltage step technique was used to measure leakage currents, as opposed to the voltage ramp technique. In the step technique, a voltage is applied to the sample and current flow into the capacitor is measured over time. At relatively short times this measurement is dominated by a charging current, while at longer times this measurement is dominated by the true steady-state leakage current.[2] This measurement is most accurate if conducted over a large enough time for the capacitor to be charged and the steady-state leakage to be measured. In the case of BZN, the steady-state regime occurs on the order of tens of seconds. This current vs. time measurement was repeated for a sequence of voltages.

2.4 References

1. W. Ren, S. Trolier-McKinstry, C.A. Randall and T.R. Shrout, "Bismuth Zinc Niobate Pyrochlore Dielectric Thin Films for Capacitive Applications," *J. Appl. Phys.* **89** (1) 767-74 (2001).

2. C. Basceri, "Electrical and Dielectric Properties of (Ba,Sr)TiO_3 Thin Film Capacitors for Ultra-High Density Dynamic Random Access Memories," Ph.D. Thesis, North Carolina State University, 1997.

Chapter 3

RESULTS

The following three compositions of BZN films were studied: $Bi_{1.5}Zn_{1.0}Nb_{1.5}O_7$, $Bi_{1.5}Zn_{0.5}Nb_{1.5}O_{6.5}$, and $Bi_2Zn_{2/3}Nb_{4/3}O_7$. Both $Bi_{1.5}Zn_{1.0}Nb_{1.5}O_7$ and $Bi_{1.5}Zn_{0.5}Nb_{1.5}O_{6.5}$ have the cubic pyrochlore structure, while $Bi_2Zn_{2/3}Nb_{4/3}O_7$ has the monoclinic zirconolite structure. The origin of the dielectric response was studied by measuring the low dc field properties as a function of temperature, frequency, and film thickness. The high dc field properties were also measured, as well as the effects of ac field on dielectric properties. The leakage current was measured to evaluate BZN films for use in applications such as decoupling capacitors.

3.1 Low Field: $Bi_{1.5}Zn_{1.0}Nb_{1.5}O_7$

As described in Chapter 1, data on MOD BZN thin films have been reported by Ren et al.[1] The low field dielectric properties of $Bi_{1.5}Zn_{1.0}Nb_{1.5}O_7$ measured here over a wider range of firing temperatures are seen in Figure 3-1. Good agreement was obtained with the previous report[1] for crystalline films. Films fired at 400 and 500 °C were amorphous. In this case, it was important that the measurements were made a couple of

hours after firing, as the loss tangent for the amorphous films increased with time. The increase in loss tangent could be due to the fact that the film was not fully densified, and absorbed water from the surrounding air.

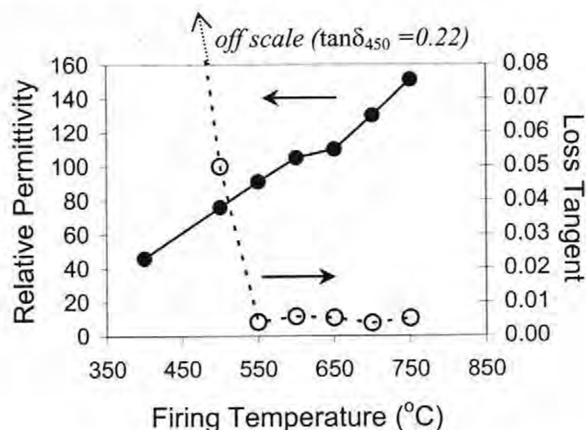

Figure 3-1: Relative permittivity and loss tangent of $Bi_{1.5}Zn_{1.0}Nb_{1.5}O_7$ films as a function of firing temperature, measured at 10 kHz and 0.03 V ac. Typical film thickness = 0.4 μm.

As described in Chapter 2, the sol-gel solution was diluted and thinner $Bi_{1.5}Zn_{1.0}Nb_{1.5}O_7$ films were made to investigate the impact of film thickness on capacitance density. Photolithography was used to pattern evaporated Au electrodes with a Cr adhesion layer between the BZN film and Au electrode. Dietz et al. reported that for $SrTiO_3$, using Au electrodes with no adhesion layer resulted in poor reproducibility and a large scatter of the experimental data that was not observed using an adhesion layer.[2]

The permittivity of these thinner films were found to be approximately thickness independent, while the loss tangent is < 0.005 for all films. For these results, photolithographically patterned 0.088 mm^2 rectangular Cr/Au top electrodes were used as the top electrode. These capacitance data were modeled as two capacitors in series to see if there is an interfacial capacitance (one capacitor is the BZN film and the other is an

interfacial capacitance that does not vary with BZN film thickness). This approach is similar to that used in $(Ba,Sr)TiO_3$ publications for high permittivity Dynamic Random Access Memories (DRAM).[3] Figure 3-2 shows the results of this analysis. The equation of the fit is shown on the plot, showing a non-zero intercept which represents the interfacial capacitance. However, the statistical error in the data is larger than the value of the intercept, so it is not conclusive that there are in fact interfacial effects. The lack of evidence of interfacial capacitance is important since as the thickness of the BZN films decreases, any interfacial capacitance will play a large role in reducing the apparent permittivity. Films thinner than 500 Angstroms would be useful, since they would improve the accuracy of the linear fit of the data.

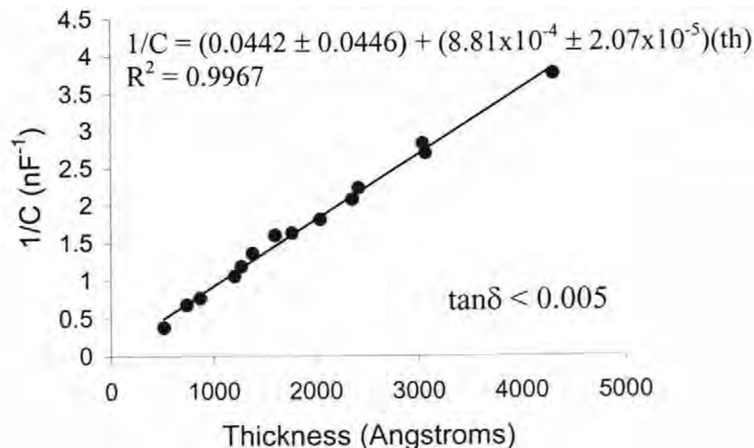

Figure 3-2: Inverse capacitance vs. thickness for $Bi_{1.5}Zn_{1.0}Nb_{1.5}O_7$.

The thickness independence of the permittivity of $Bi_{1.5}Zn_{1.0}Nb_{1.5}O_7$ is in contrast to that found in ferroelectric films such as BST. Figure 3-3 shows the permittivity of six different thicknesses of $(Ba_{0.7}Sr_{0.3})Ti_{0.53}O_3$ films as a function of field.[4] The thickness

dependence of the permittivity of BST can be noticed by comparing the zero-field permittivities for the different thicknesses of films.

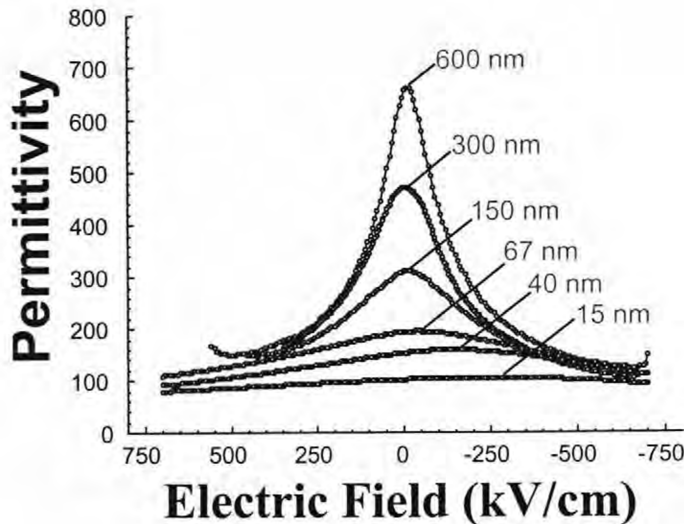

Figure 3-3: Permittivity vs. dc field for $(Ba_{0.7}Sr_{0.3})Ti_{0.53}O_3$ films, with thicknesses of 15 – 600 nm. The thin films were deposited using MOCVD.[4]

The equivalent oxide thickness is a measure of the performance of DRAM capacitor dielectrics. It is defined as the equivalent amount of SiO_2 that would generate the same capacitance per unit area. The equivalent SiO_2 thickness is given by $(\varepsilon_s/\varepsilon_{BZN})*t$, where t is the thickness of BZN, and ε_s and ε_{BZN} are the low field relative permittivities of SiO_2 and $Bi_{1.5}Zn_{1.0}Nb_{1.5}O_7$, respectively. This calculation was done using the data from Figure 3-2; the results are shown in Figure 3-4. At 520 Angstroms, this is approximately twice as thick as the equivalent oxide thickness of $(Ba_{0.75}Sr_{0.25})TiO_3$.[5]

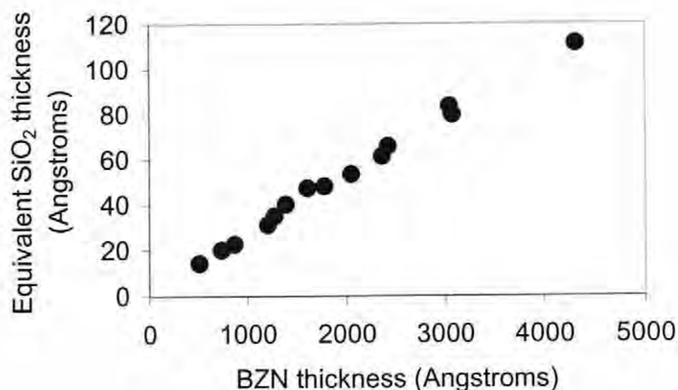

Figure 3-4: Equivalent oxide thickness for $Bi_{1.5}Zn_{1.0}Nb_{1.5}O_7$ films.

3.2 A New Cubic Composition: $Bi_{1.5}Zn_{0.5}Nb_{1.5}O_{6.5}$

As described in Chapter 1 (Section 1.1), the role of reducing the Zn content in $Bi_{1.5}Zn_{1.0}Nb_{1.5}O_7$ ceramics was studied by Nino.[6] Although $Bi_{1.5}Zn_{0.92}Nb_{1.5}O_{6.92}$ was proposed as the stoichiometry of cubic pyrochlore, through analyzing the lattice parameter of cubic pyrochlore it was reported that the amount of Zn can be reduced to 0.84 without resulting in a second phase of $BiNbO_4$.[6] For thin films however, it was thought that it might be possible to reduce the amount of Zn without secondary phases forming, so the properties of cubic BZN batched to have zero Zn on the A-site were explored. As a result, MOD solutions were made with the composition $Bi_{1.5}Zn_{0.5}Nb_{1.5}O_{6.5}$. In this section, the dielectric properties of $Bi_{1.5}Zn_{0.5}Nb_{1.5}O_{6.5}$ MOD films are reported and compared with the properties of $Bi_{1.5}Zn_{1.0}Nb_{1.5}O_7$ and $Bi_2Zn_{2/3}Nb_{4/3}O_7$.

3.2.1 Thermal Analysis

A $Bi_{1.5}Zn_{0.5}Nb_{1.5}O_{6.5}$ MOD solution was heated to 120 °C for 2 hours, to remove some of the liquid organics, resulting in a gel. Differential thermal analysis (DTA) was performed on this gel, with the results shown in Figure 3-5. The DTA curve shows two exothermic peaks at 360 and 540 °C. The exothermic peak at 360 °C corresponds with the decomposition of most of the organics in the gel. The exothermic peak at 540 °C corresponds to crystallization of the BZN. As expected, this DTA curve is comparable to that of $Bi_{1.5}Zn_{1.0}Nb_{1.5}O_7$ and $Bi_2Zn_{2/3}Nb_{4/3}O_7$.[1]

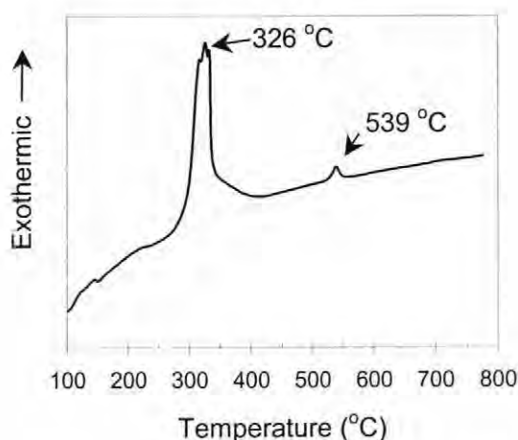

Figure 3-5: DTA curve of $Bi_{1.5}Zn_{0.5}Nb_{1.5}O_{6.5}$ MOD solution.

3.2.2 Crystallization

Figure 3-6 shows the XRD patterns of $Bi_{1.5}Zn_{0.5}Nb_{1.5}O_{6.5}$ films fired at different temperatures. There were no sharp diffraction peaks for films fired at 500 °C and below, signifying amorphous films. Corroborating the DTA data, films fired at 550 °C were crystalline and showed a cubic pyrochlore structure. The films showed the cubic

pyrochlore structure through 650 °C firing temperatures. When fired at 700 °C, the films decomposed into $BiNbO_4$ and cubic pyrochlore. This is in contrast to cubic $Bi_{1.5}Zn_{1.0}Nb_{1.5}O_7$, which does not decompose at temperatures less than 800 °C.[1]

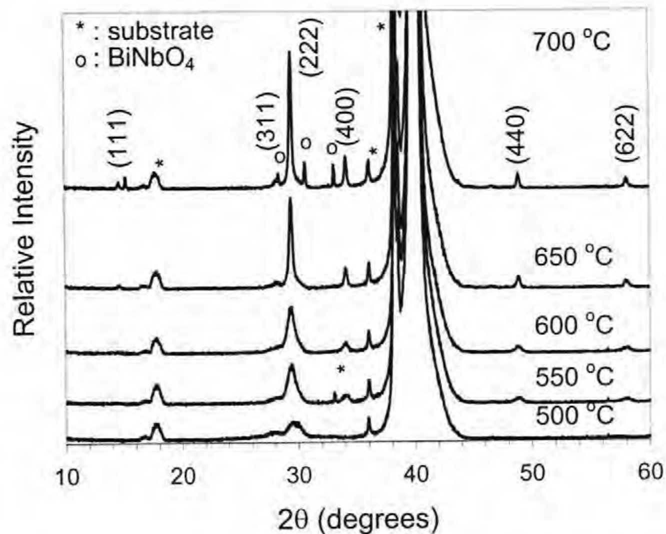

Figure 3-6: XRD patterns of $Bi_{1.5}Zn_{0.5}Nb_{1.5}O_{6.5}$ films fired at different temperatures.

3.2.3 Low Field: $Bi_{1.5}Zn_{0.5}Nb_{1.5}O_{6.5}$

Figure 3-7 shows the permittivity and loss tangent of BZN thin films as a function of firing temperature; data for $Bi_{1.5}Zn_{1.0}Nb_{1.5}O_7$ and $Bi_2Zn_{2/3}Nb_{4/3}O_7$ agree with those reported by Ren et al.[1] The permittivity of $Bi_{1.5}Zn_{0.5}Nb_{1.5}O_{6.5}$ increased with firing temperature, reaching a maximum of 180 at 600 – 650 °C. At 700 °C, the decrease in permittivity is reasonable since, as determined by XRD, the film decomposes into $BiNbO_4$ and cubic pyrochlore. $BiNbO_4$ has a lower permittivity of 42 with loss tangent < 0.005.[7] As described by Ren et al.,[1] the permittivity and loss of $Bi_{1.5}Zn_{1.0}Nb_{1.5}O_7$ and $Bi_2Zn_{2/3}Nb_{4/3}O_7$ MOD thin films compared favorably with bulk ceramics of the same

composition. However, phase-pure bulk samples of $Bi_{1.5}Zn_{0.5}Nb_{1.5}O_{6.5}$ were not, to date, prepared for comparison.[6] Similar to the other two BZN compositions,[1] the loss tangent was low (<0.005).

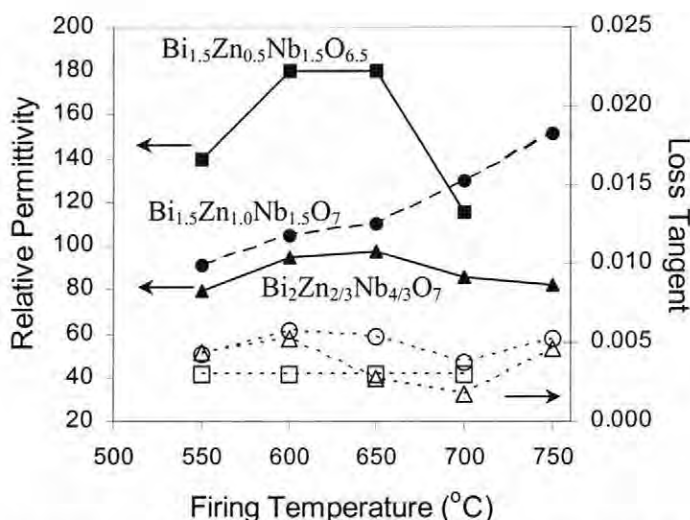

Figure 3-7: Relative permittivity and loss tangent of BZN films at different firing temperatures, measured at 10 kHz and 0.03 V ac.

The Temperature Coefficient of Capacitance (TCC) for films fired at different temperatures was calculated over the measuring temperature range of 100 to –50 °C by:

$$TCC = \frac{1}{C}\frac{\partial C}{\partial T} \qquad (3.1)$$

where C is capacitance and T is temperature. The TCCs of $Bi_{1.5}Zn_{0.5}Nb_{1.5}O_{6.5}$ films fired at various temperatures are shown in Figure 3-8, along with the TCCs of $Bi_{1.5}Zn_{1.0}Nb_{1.5}O_7$ and $Bi_2Zn_{2/3}Nb_{4/3}O_7$ films, which agree with those reported by Ren et al.[1] As with $Bi_{1.5}Zn_{1.0}Nb_{1.5}O_7$ and $Bi_2Zn_{2/3}Nb_{4/3}O_7$,[1] the permittivity of $Bi_{1.5}Zn_{0.5}Nb_{1.5}O_{6.5}$ changed linearly with temperature over this range. It is important to

notice that the maximum permittivity of $Bi_{1.5}Zn_{0.5}Nb_{1.5}O_{6.5}$ occurs when fired at 600 – 650 °C, so the TCC for the processing temperature of the maximum permittivity is actually lower than for cubic $Bi_{1.5}Zn_{1.0}Nb_{1.5}O_7$ at its temperature of maximum permittivity. It would be interesting to examine whether $Bi_{1.5}Zn_{0.5}Nb_{1.5}O_{6.5}$ films fired at 600 °C to 650 °C are fully crystallized, or whether there is residual amorphous material. Transmission Electron Microscopy (TEM) would be useful in identifying whether this is, in fact, the case.

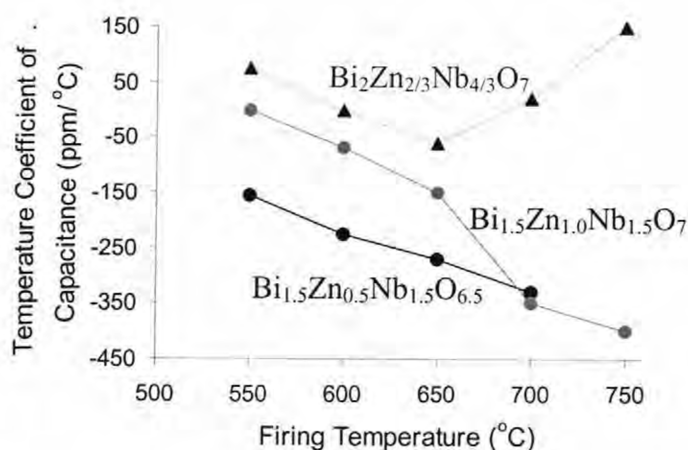

Figure 3-8: TCC of BZN films at different firing temperatures.

Similar to cubic pyrochlore $Bi_{1.5}Zn_{1.0}Nb_{1.5}O_7$ ceramics[6,8] and films,[1] cubic pyrochlore $Bi_{1.5}Zn_{0.5}Nb_{1.5}O_{6.5}$ films also showed a low temperature dielectric relaxation. Figure 3-9 shows the permittivity and loss of $Bi_{1.5}Zn_{0.5}Nb_{1.5}O_{6.5}$ films fired at 600 °C as a function of measuring temperature, along with data for $Bi_{1.5}Zn_{1.0}Nb_{1.5}O_7$ films fired at 750 °C for comparison. The data for $Bi_{1.5}Zn_{1.0}Nb_{1.5}O_7$ agree with those reported by Ren et al.[1] Frequency dispersion in the dielectric properties was observed in

$Bi_{1.5}Zn_{0.5}Nb_{1.5}O_{6.5}$ with the permittivity dropping 33 % at 4 K from its maximum value, compared to a decrease of 50 % for $Bi_{1.5}Zn_{1.0}Nb_{1.5}O_7$. As with $Bi_{1.5}Zn_{1.0}Nb_{1.5}O_7$, the maxima in the permittivity curves decrease and shift to higher temperature with increasing measuring frequency. The corresponding maxima of loss tangents increase and shift to higher temperature with increasing frequency. However, the onset of relaxation occurs 30 - 50 K lower in temperature. This should expand the frequency range over which $Bi_{1.5}Zn_{0.5}Nb_{1.5}O_{6.5}$ can be used (relative to $Bi_{1.5}Zn_{1.0}Nb_{1.5}O_7$) without the shoulder of the loss curve impinging at the operating temperatures of potential higher frequency applications.

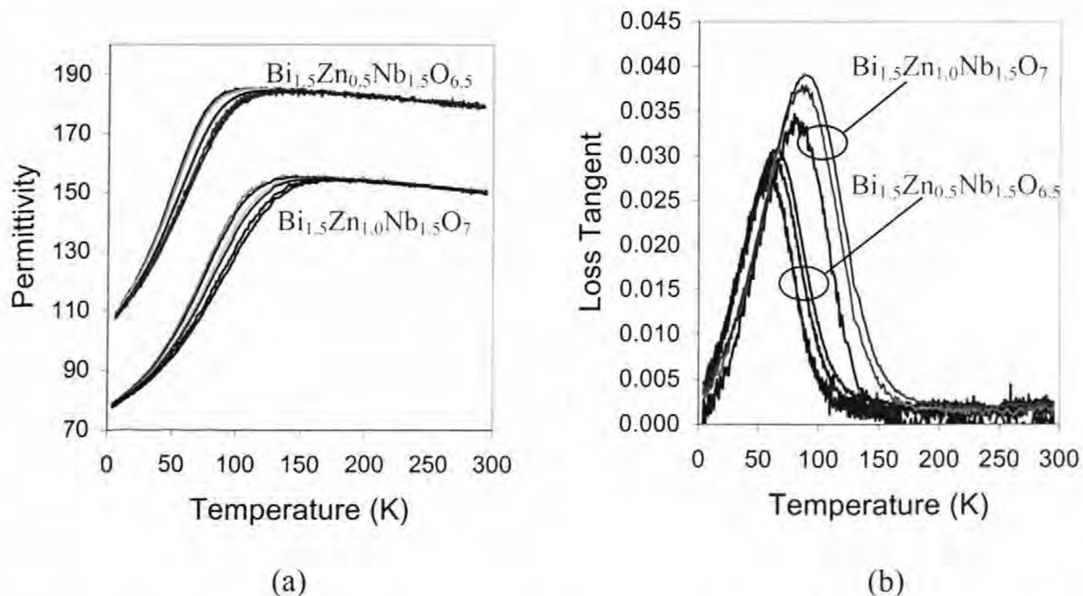

Figure 3-9: (a) Permittivity and (b) loss of $Bi_{1.5}Zn_{0.5}Nb_{1.5}O_{6.5}$ films (fired at 600 °C) and $Bi_{1.5}Zn_{1.0}Nb_{1.5}O_7$ films (fired at 750 °C) as a function of measuring temperature. For each composition, the frequency changes from the top curve to the bottom curve in the order: 0.5, 1, 5, 10, 50, 100 kHz for permittivity; 10, 5, 1 kHz for the loss tangent.

Similar to $Bi_{1.5}Zn_{1.0}Nb_{1.5}O_7$,[1] the maximum in the loss tangent for $Bi_{1.5}Zn_{0.5}Nb_{1.5}O_{6.5}$ can be fitted to an Arrhenius equation (Equation 1.1). Figure 3-10 shows the fit for $Bi_{1.5}Zn_{0.5}Nb_{1.5}O_{6.5}$ films based on the loss tangent data presented in Figure 3-9. E_a and υ_o calculated using Equation 1.1 were 0.11 ± 0.0054 eV and $4.57 \times 10^{12} \pm 2.86$ Hz, respectively. The jump frequency υ_o of $Bi_{1.5}Zn_{0.5}Nb_{1.5}O_{6.5}$ films had approximately the same order of magnitude as ionic vibrations of the lattice (~10^{13} Hz), and values for both E_a and υ_o were comparable to that reported for $Bi_{1.5}Zn_{1.0}Nb_{1.5}O_7$ thin films[1] and $Bi_{1.5}Zn_{1.0}Nb_{1.5}O_7$ ceramics by Nino et al.[8] and Kamba et al.[9] This Arrhenius behavior contrasts with that of ferroelectric relaxors like PMN-PT,[10] spin glasses,[11] and some dipole glasses[12] which follow the Vogel-Fulcher equation (Equation 1.2).

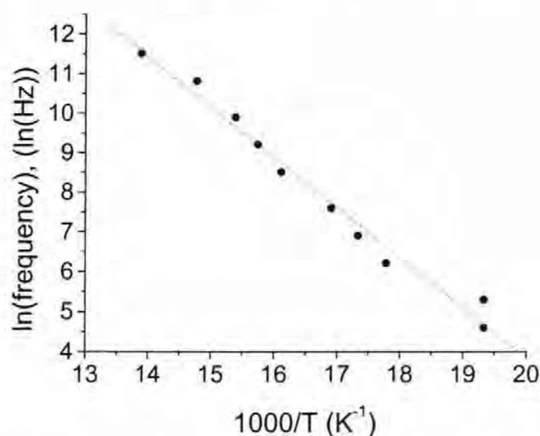

Figure 3-10: Arrhenius plot of $Bi_{1.5}Zn_{0.5}Nb_{1.5}O_{6.5}$ based on curve-fit data in Figure 3-9b.

From the work of Nino,[6] the increase in permittivity of $Bi_{1.5}Zn_{0.5}Nb_{1.5}O_{6.5}$ over $Bi_{1.5}Zn_{1.0}Nb_{1.5}O_7$ cannot be completely explained by the removal of a ZnO second phase, as was originally hypothesized. Rather, it is likely that in films, as in ceramics, at least

some of the Zn occupies the A-site in $Bi_{1.5}Zn_{1.0}Nb_{1.5}O_7$, (since $Bi_{1.5}Zn_{0.92}Nb_{1.5}O_{6.95}$ ceramic was found to not have any ZnO second phase). One possible explanation as to why the permittivity is higher in $Bi_{1.5}Zn_{0.5}Nb_{1.5}O_{6.5}$ than in $Bi_{1.5}Zn_{1.0}Nb_{1.5}O_7$ could be due to the increase in vacancies present in $Bi_{1.5}Zn_{0.5}Nb_{1.5}O_{6.5}$. An increased number of vacancies might lead to higher permittivity, either because of increased polarizability due to the additional space, or since the Bi my experience different random fields.

3.3 High dc Field

In order to use BZN films in tunable applications, their behavior under high dc fields must be characterized. The effects of dc fields on permittivity, as well as polarization, of BZN films will be described in this Section.

3.3.1 High dc Field: $Bi_{1.5}Zn_{1.0}Nb_{1.5}O_7$

Figure 3-11 shows the permittivity and loss of $Bi_{1.5}Zn_{1.0}Nb_{1.5}O_7$ as a function of applied dc field, using 0.03 V ac. This measurement was made starting at zero dc bias, increasing to the maximum positive field, decreasing to the maximum negative field, and returning to zero. No hysteresis was observed since the data from each cycle can be superimposed, within experimental error. The tunability of the permittivity of $Bi_{1.5}Zn_{1.0}Nb_{1.5}O_7$, using Equation 1.3, is 30 % at 1.8 MV/cm when measured at room temperature. The measurement was repeated at liquid nitrogen temperature, 77 K, since

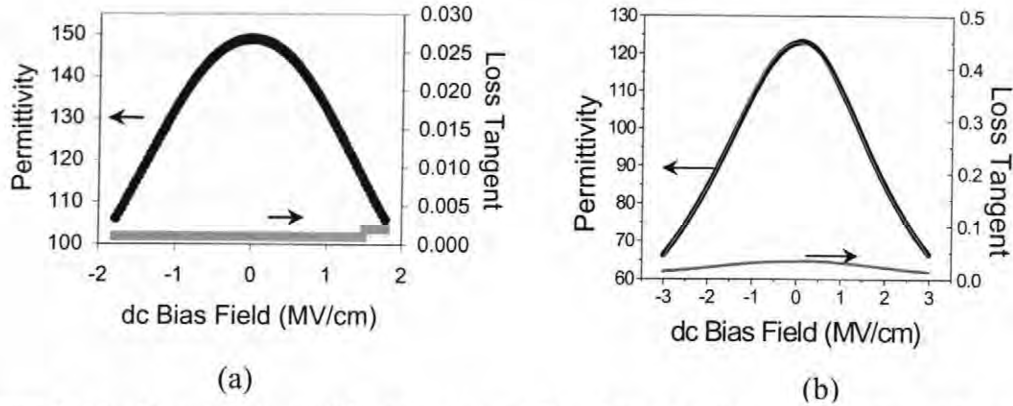

Figure 3-11: Permittivity and loss tangent of $Bi_{1.5}Zn_{1.0}Nb_{1.5}O_7$ as a function of applied dc field, measured at 10 kHz and 0.03 V ac. (a) 300 K, (b) 77 K.

the decrease in electronic conduction at lower temperatures enables higher fields to be applied without breakdown being an issue. Using a figure of merit defined as: [13]

$$FOM = (Q_{zero\ field})(\%\ tunability) \tag{3.2}$$

at room temperature and 1.8 MV/cm, $Bi_{1.5}Zn_{1.0}Nb_{1.5}O_7$ has a FOM of 5900.

The tunability of $Bi_{1.5}Zn_{1.0}Nb_{1.5}O_7$ at 77 K is 45 % at 3.0 MV/cm, with a FOM of 3400. When comparing the tunability data measured at different temperatures, it is important to notice that the permittivity at 77 K is lower than at 300 K due to the dielectric relaxation shown in Figure 3-9. At higher fields (Figure 3-11b), the slope of the curve begins to decrease, showing saturation of the polarization. The highest field data were fit to a power series expansion of the even terms of the applied field:

$$\varepsilon_r = (123\pm0.0937) - (14.7\pm0.125)E^2 + (1.56\pm0.0374)E^4 - (0.0690\pm0.00296)E^6 \tag{3.3}$$

where ε_r is the permittivity and E is the applied dc field (in MV/cm), $R^2 = 0.9992$. The odd terms were not used for fitting; since $Bi_{1.5}Zn_{1.0}Nb_{1.5}O_7$ has cubic symmetry the coefficients of the odd-powered terms are zero.[6,8]

The tunability of permittivity with an applied dc field was measured on the thinner $Bi_{1.5}Zn_{1.0}Nb_{1.5}O_7$ films shown in Figure 3-2 with Cr/Au top electrodes; the results for measurements made at 77 K are shown in Figure 3-12. For all of the thicknesses measured, ≥ 520 Angstroms, the 21 % tunability at 1.5 MV/cm is the same as that found for the 0.52 μm film in Figure 3-11b. Thus, unlike many $(Ba,Sr)TiO_3$ capacitors,[3,4] there appears to be no thickness dependence of the tunability. The slight hysteresis in Figure 3-12 is due to the top and bottom electrodes being different metals, and is not intrinsic to $Bi_{1.5}Zn_{1.0}Nb_{1.5}O_7$. The effects of different electrode materials will be explored in more detail in Section 3.5.

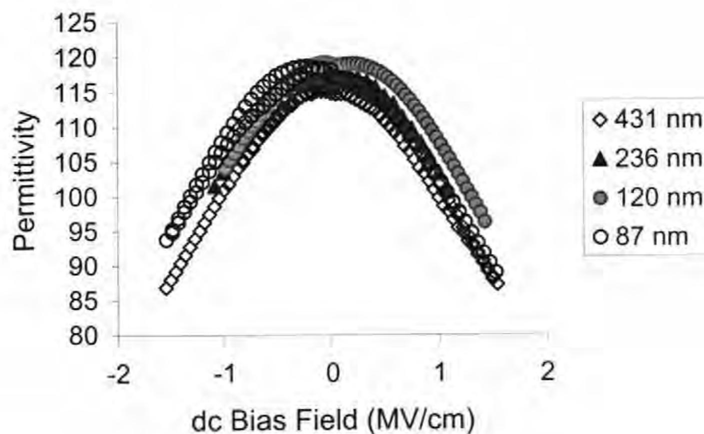

Figure 3-12: Permittivity of $Bi_{1.5}Zn_{1.0}Nb_{1.5}O_7$ with applied dc field for varying thicknesses of films with Cr/Au top electrodes, measured at 10 kHz, 0.03 V ac, and 77 K. Loss tangent ≤ 0.04.

Figure 3-3 was used in Section 3.1 to compare the zero-field permittivity of $Bi_{1.5}Zn_{1.0}Nb_{1.5}O_7$ with BST. The tunabilities of $Bi_{1.5}Zn_{1.0}Nb_{1.5}O_7$ and BST can also be compared using Figure 3-3. First, it is important to note that the tunability of BST decreases with decreasing thickness. Also, the permittivity (and capacitance density) of BST decreases under significantly lower fields than $Bi_{1.5}Zn_{1.0}Nb_{1.5}O_7$. This is important for some applications that operate at a specific operating voltage, since as the thickness of the films decrease the field they operate under increases.

3.3.2 High dc Field: $Bi_{1.5}Zn_{0.5}Nb_{1.5}O_{6.5}$

The permittivity and loss as a function of applied dc field is shown in Figure 3-13. As expected, $Bi_{1.5}Zn_{0.5}Nb_{1.5}O_{6.5}$ has similar tunability as $Bi_{1.5}Zn_{1.0}Nb_{1.5}O_7$ at the same field: 26 % at 1.8 MV/cm, with a 77 K FOM of 1800 (Equation 3.2). The measurement was made at 77 K since higher fields could be applied at 77 K than at room temperature. Also similar to $Bi_{1.5}Zn_{1.0}Nb_{1.5}O_7$, no hysteresis was observed.

$Bi_{1.5}Zn_{0.5}Nb_{1.5}O_{6.5}$ also follows a similar fitting equation as Equation 3.3, over the field range measured:

$$\varepsilon_r = (184 \pm 0.0692) - (18.5 \pm 0.156)E^2 + (1.16 \pm 0.0818)E^4 + (0.107 \pm 0.0111)E^6 \quad (3.4)$$

where ε_r is the permittivity and E is the applied dc field (in MV/cm). It is possible that the difference in the sign of the E^6 term between Equations 3.3 and 3.4 is simply due to data for $Bi_{1.5}Zn_{0.5}Nb_{1.5}O_{6.5}$ not going to high enough field to see the saturation in the polarization. More data at higher fields would be necessary to definitely clarify the magnitudes of all coefficients.

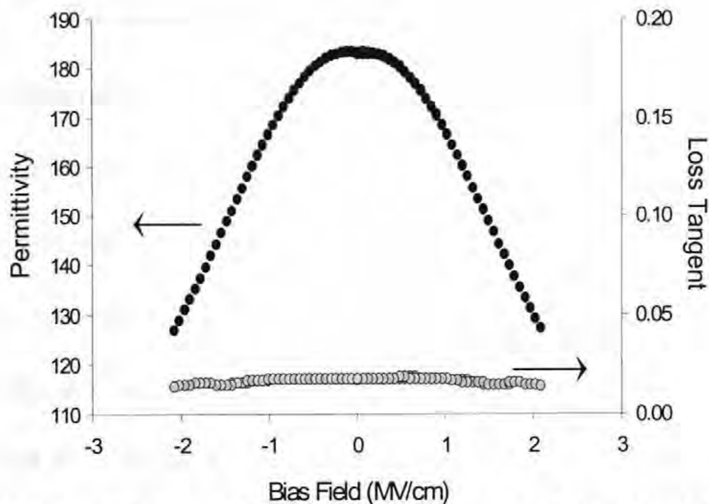

Figure 3-13: Permittivity and loss tangent of $Bi_{1.5}Zn_{0.5}Nb_{1.5}O_{6.5}$ films as a function of applied dc field, measured at 10 kHz, 0.03 V ac, and 77 K.

From the work of Nino,[6] the difference in the structure between the two compositions is expected to be the amount of Zn on the A-site (the amount of Zn on the B-site is 0.5 mole in both cases). The A-site occupancy affects the polarizability of BZN, since $Bi_{1.5}Zn_{0.5}Nb_{1.5}O_{6.5}$ has a higher permittivity than $Bi_{1.5}Zn_{1.0}Nb_{1.5}O_7$ (180 and 150, respectively). However, from the similarity in tunability between $Bi_{1.5}Zn_{1.0}Nb_{1.5}O_7$ and $Bi_{1.5}Zn_{0.5}Nb_{1.5}O_{6.5}$, it can be concluded that the amount of Zn on the A-site does not affect the higher order polarizability of BZN.

In order to compare BST and BZN for use in applications such as decoupling capacitors, it is important to examine the capacitance density of the films as a function of thickness. Figure 3-14 shows this comparison for $Bi_{1.5}Zn_{1.0}Nb_{1.5}O_7$, $Bi_{1.5}Zn_{0.5}Nb_{1.5}O_{6.5}$ (labeled BZN-1 and BZN-0.5, respectively), and the $(Ba_{0.7}Sr_{0.3})Ti_{0.53}O_3$ films shown in Figure 3-3. Since applications such as decoupling capacitors operate with a field applied, Figure 3-14 shows the capacitance densities when 5 V or 1 V are applied. The data for BST were calculated directly from Figure 3-3. Since BZN does not show a thickness

dependence of permittivity (see Figure 3-2) or tunability (see Figure 3-12), the field for a specific thickness was determined, and then the capacitance density was calculated from Figures 3-11 and 3-13.

The results shown in Figure 3-14 are reasonable since due to its higher permittivity, $Bi_{1.5}Zn_{0.5}Nb_{1.5}O_{6.5}$ has a higher capacitance density than $Bi_{1.5}Zn_{1.0}Nb_{1.5}O_7$. Also, at smaller thicknesses it is reasonable that BST has a lower capacitance density than BZN since it shows a dramatic decrease in permittivity with thickness, while BZN does not show any thickness dependence. Also, as mentioned above, the capacitance of BST decreases more than BZN under similar fields. From Figure 3-14, BZN shows potential for use in applications, especially ones that require small thickness films.

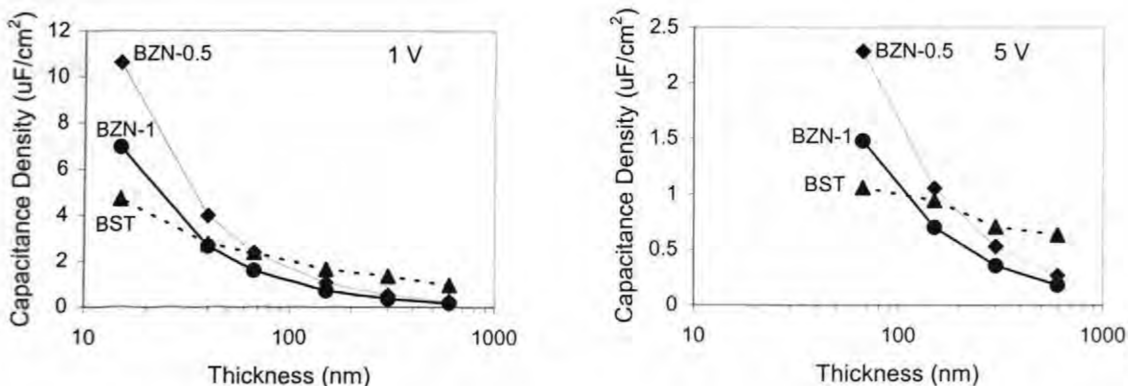

Figure 3-14: Plots of capacitance density vs. thickness of films comparing $Bi_{1.5}Zn_{1.0}Nb_{1.5}O_7$, $Bi_{1.5}Zn_{0.5}Nb_{1.5}O_{6.5}$, and $(Ba_{0.7}Sr_{0.3})Ti_{0.53}O_3$ (BZN-1, BZN-0.5, and BST, respectively). (a) 1 V dc applied, (b) 5 V dc applied.

3.3.3 High dc Field: $Bi_2Zn_{2/3}Nb_{4/3}O_7$

Ren et al. reported measuring the permittivity of $Bi_2Zn_{2/3}Nb_{4/3}O_7$ while applying a dc field (-830 kV/cm to 830 kV/cm) and found little field dependence of the

permittivity.[1] Figure 3-15 shows that when higher fields are applied, the permittivity of $Bi_2Zn_{2/3}Nb_{4/3}O_7$ is definitely tunable. This measurement was made at 77 K since higher fields can be applied, as described above; the maximum tunability is 20 % at 4.0 MV/cm. Modifying Equation 3.2 to define ε_r as the maximum permittivity, the FOM for $Bi_2Zn_{2/3}Nb_{4/3}O_7$ is 9300 at 4.0 MV/cm. The increase in loss tangent at high fields is due to increased conduction at high voltages. The measurements followed the same procedure as described above for $Bi_{1.5}Zn_{1.0}Nb_{1.5}O_7$; $Bi_2Zn_{2/3}Nb_{4/3}O_7$ also showed little hysteresis. The fact that the permittivity increases and then decreases as the field changes from zero could be due to a field-induced ordering of Zn atoms within the hexagonal tungsten bronze layer in the zirconolite structure[14] (see Figure 1-2). However, attempts to measure the polarization-electric field hysteresis loop at 77 K showed no evidence of a remanent polarization, for fields of ± 4 MV/cm. This suggests that it is not possible to induce long-range ordering with these field levels.

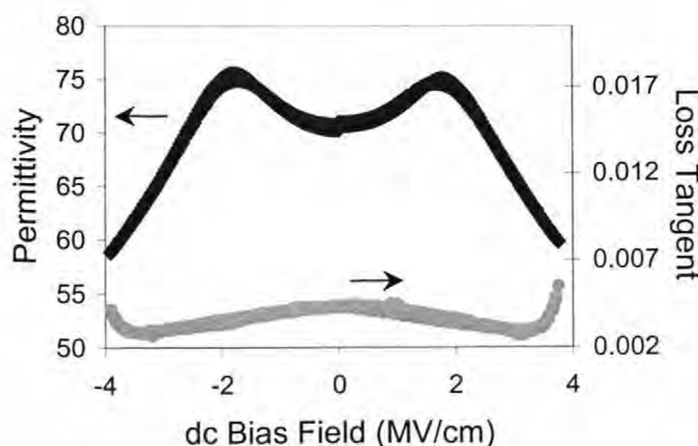

Figure 3-15: Permittivity and loss tangent of $Bi_2Zn_{2/3}Nb_{4/3}O_7$ as a function of applied dc field, measured at 10 kHz, 0.03 V ac, and 77 K.

3.3.4 Polarization-Field Measurements

The polarization as a function of applied dc field can be calculated from the tunability seen in the permittivity vs. dc field curves (Figs. 3-11 and 3-13) according to the following equation:

$$P(V) = \frac{1}{A}\int C(V)\,dV \qquad (3.5)^{15}$$

where P is polarization, C is capacitance, A is the area of electrode, and V is dc voltage. Using Equation 3.5 and the data from Figures 3-11 and 3-13, the calculated P-E curves are shown in Figures 3-16 and 3-17, respectively, measured under quasistatic conditions, along with the measured polarization using a Sawyer-Tower circuit at 0.5 Hz.

A study was made of the ac field tunability of BZN to examine if this difference between the integrated C-V curves and the measured P-E data could be explained by the effect of ac oscillation voltage on the permittivity, as described in the next section.

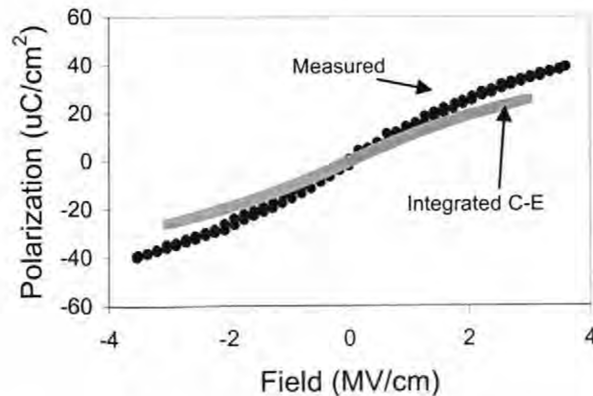

Figure 3-16: P-E curves for $Bi_{1.5}Zn_{1.0}Nb_{1.5}O_7$, showing both measured and integrated C-E data from Figure 3-11b, 77 K.

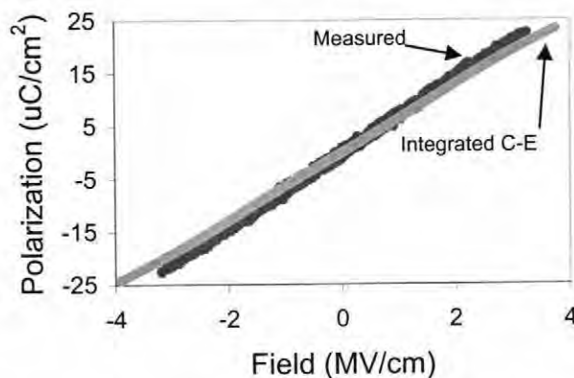

Figure 3-17: P-E curves for $Bi_2Zn_{2/3}Nb_{4/3}O_7$, showing both measured and integrated C-E data from Figure 3-14, 77 K.

3.4 ac Field Tunability of BZN

In addition to dc tunability, it was found that the three compositions of BZN films that were studied showed an ac field dependence of the permittivity. Figure 3-18 shows that under low ac fields, both the permittivity and loss tangent increase with increasing ac field for $Bi_2Zn_{2/3}Nb_{4/3}O_7$ (< 1 % change in permittivity at 500 kV/cm). Although it is possible that this increase in permittivity is due to heating, it is not likely since it can be calculated that this increase in permittivity would result in 30 °C increase in temperature.[1] This much of an increase in temperature is not expected since the loss tangent in Figure 3-18 does not increase significantly.

Figure 3-19 shows the same measurement for $Bi_{1.5}Zn_{0.5}Nb_{1.5}O_{6.5}$, measured at different points in the relaxation, 77 K and 300 K. The permittivity and loss tangent of this cubic composition also increases, with the permittivity showing larger tunability (5-6 % at 500 kV/cm) than $Bi_2Zn_{2/3}Nb_{4/3}O_7$, coupled with a larger increase in the loss tangent. The fact that the permittivity increases at both measuring temperatures indicates that this

increase in permittivity is not simply due to heating since at 300 K the permittivity would decrease slightly with increasing temperature (see Figure 3-9a).

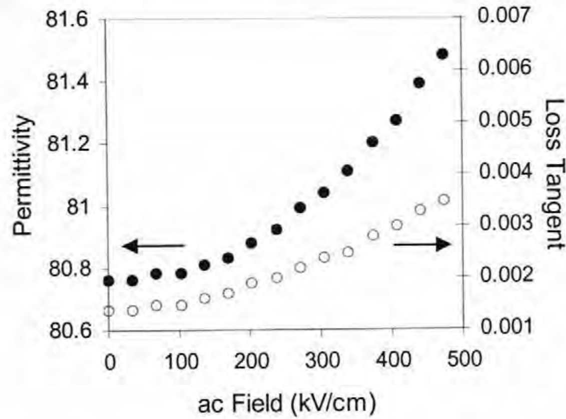

Figure 3-18: Permittivity and loss tangent of $Bi_2Zn_{2/3}Nb_{4/3}O_7$ films as a function of applied ac field, measured at 10 kHz, 300 K.

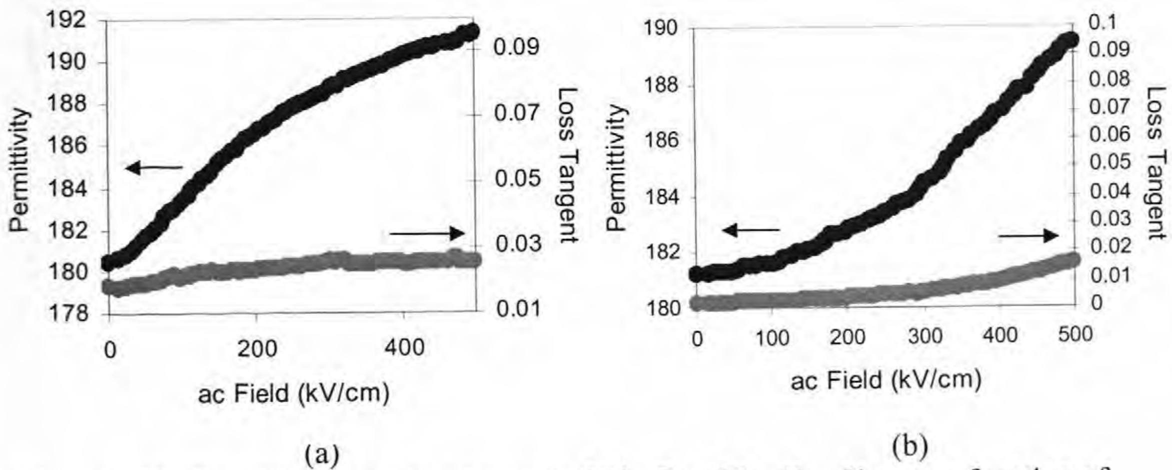

Figure 3-19: Permittivity and loss tangent of $Bi_{1.5}Zn_{0.5}Nb_{1.5}O_{6.5}$ films as a function of applied ac field, measured at 10 kHz. (a) 77 K, (b) 300 K.

To fully describe the effect of ac field on the permittivity of BZN, however, higher field data would be necessary.

Through studying the relaxation of cubic BZN, as well as the ac and dc field tunability, it can be concluded that the currently predominant models of ferroelectric relaxors described in Chapter 1 are not adequate in describing BZN. For example, models such as superparaelectric and dipole glass would predict similar tunability behavior for both ac and dc fields.[16] However, as described above, the permittivity decreases under dc field and increases under ac field. The breathing model proposed by Glazounov and Tagantsev predicts differing behaviors such as these for PMN.[16] However, since BZN is not ferroelectric it is not clear what the corollary is to domain wall motion and spontaneous polarization. However, the model of relaxation proposed by Nino for BZN ceramics[6] may also apply to BZN thin films. It attributes the relaxation to a jump from one energy potential well to another over an energy barrier associated with the activation energy. This activation energy can be calculated from the Arrhenius behavior. Within each energy well, there are smaller jumps possible due to multiple states that are thermodynamically equivalent. These smaller jumps are dictated by random fields that result from phenomena such as site disorder.[6]

3.5 Leakage Current

Low leakage currents are necessary if BZN films are going to be incorporated into commercial applications.[17,18] For example, BZN films would be exposed to high dc fields in applications such as high frequency tunable devices. Leakage currents can also decrease the effectiveness of decoupling capacitors since high capacitance density films

can experience high fields[19] (e.g. a 30 nm thick capacitor exposed to a 1 V bias is under a field of 330 kV/cm).

3.5.1 Leakage Current: Background

When a dc electric field is applied to metal-insulator-metal (MIM) structures, species such as electrons, holes, and ions may migrate, leading to a current.[20] It is important to examine the current-voltage characteristics of BZN films in order to identify the rate-limiting transport mechanism. This knowledge can lead to an understanding of the material properties of the insulator and contacts. Two characteristics of current transport in insulating films are that the current density (J) vs. dc field (E) behavior is typically non-ohmic, and conduction mechanisms are thermally activated, with the exception of tunneling (described later).[20]

Many groups have investigated conduction mechanisms in various perovskite thin films, including $SrTiO_3$, BST, and $Pb(Zr,Ti)O_3$.[2, 3, 21-36] Transport mechanisms which dominate behavior in MIM structures can be grouped into two general categories: bulk-limited and interface-limited (often with one of the interfaces, or electrodes, dominating).[20] Four of the models that apply to rate-limiting transport mechanisms are (1) tunneling, (2) space-charge-limited currents (SCLC), (3) Poole-Frenkel, and (4) thermionic emission. These models are described below:[37-44]

(1) Tunneling: electrons may tunnel through thin barriers (usually <10 nm) even when the electron energy is smaller than the barrier height.[36] (see Figure 3-20) Under high voltages, interface energy barriers can become thin, leading to Fowler-Nordheim

emission in which tunneling takes place through the thinned interface energy barrier. Tunneling is typically independent of temperature:[45]

$$J_{FN} = \frac{q^3E^2}{16\pi^2 h\phi} \exp\left[-\frac{\pi\, m^{1/2}\ \phi^{3/2}}{2\sqrt{2}\ qhE}\right] \qquad (3.6)^{46}$$

where q is the charge of an electron, *h* is Planck's constant, m is the effective mass of the tunneling electron, E is the electric field, and ϕ is the tunneling barrier height.

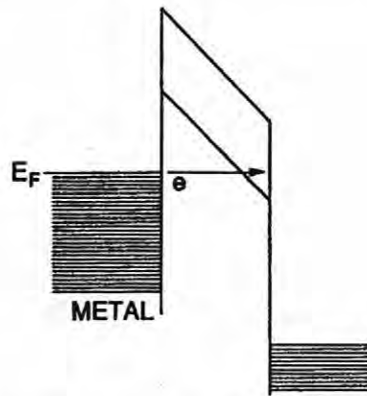

Figure 3-20: Schematic of tunneling conduction mechanism.[20]

(2) SCLC: In the case of an ohmic contact, SCLC occurs above a critical voltage:

$$J_{SCL} = \frac{9\mu\varepsilon}{8d}E^2 \qquad (3.7)^{20}$$

where μ is mobility, ε is permittivity of the dielectric, d is film thickness, and E is electric field (see Figure 3-21a). This equation has been modified based upon the trap characteristics in films.[21,22,30,37] SCLC is bulk limited since it occurs when contacts easily allow injection, with the current flow limited by space charge that forms from the high rate of injected electrons.[37] High rates of injection can be caused either by contacts with

a low barrier height that lead to easy thermionic emission, or thin barriers that lead to easy tunneling. Due to these conditions, SCLC is unlikely to be rate-limiting for metal contacts on wide bandgap semiconductors or insulators.[37] Current flow does not depend on the contact material if the interface barrier is low enough to allow sufficient charge carrier emission.[2] The current-voltage behavior is ohmic at low voltages, where there is a lower rate of charge carrier emission from electrodes than thermionically generated in the bulk. The current-voltage behavior follows Equation 3.7 at higher voltages, with the starting voltage of this behavior strongly dependent on the trap density in the film.[2]

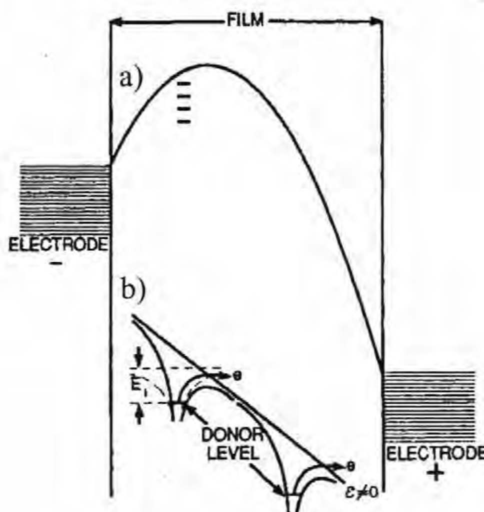

Figure 3-21: (a)Space charge-limited, and (b)Poole-Frenkel mechanisms of conduction.[20]

(3) Poole-Frenkel effect: The leakage of films which show hopping conduction of electronic carriers depends on the equilibrium between trapped and free carriers (see Figure 3-21b). Applying an electric field can lower the barrier at the traps. Replenishing contacts are required to maintain steady state conditions.[22] Thermionic emission of

charge carriers out of these traps can be described by: $\Delta W_{PF} = q\sqrt{\frac{qE}{\pi\varepsilon}}$, where W indicates an energy barrier height, ε the permittivity of the dielectric, E the electric field, and q the charge.[2] This leads to the field dependence of the current density[36]

$$J_{PF} \propto E \exp\left(-\frac{1}{kT}\left(W_{tr} - \Delta W_{PF}\right)\right) \qquad (3.8)^{2}$$

where W_{tr} is the depth of the energy trap.

(4) Thermionic emission: For an electron transfer, charge carriers need enough energy to overcome an energy barrier, W_B, assuming the barrier is thick enough to avoid tunneling (see Figure 3-22). The temperature dependence of the thermionic emitted current density is $J_{TE} = AT^2 \exp\left(-\frac{W_B}{kT}\right)$ where W_B is the height of the energy barrier, and A is the effective Richardson constant.[2] The barrier can be lowered by mechanisms such as the Schottky effect, which effectively reduces the work function:[45]

$$J_S = AT^2 \exp\left(-\frac{qW_B}{kT}\right) \exp\left[\frac{q}{kT}\left(\frac{q}{4\pi\varepsilon}E\right)^{\frac{1}{2}}\right] \qquad (3.9)^{20}$$

where W_B is the height of the energy barrier, A is the effective Richardson constant, q the charge, E the electric field, and ε the permittivity of the dielectric.

As mentioned in Chapter 2, it is important to separate the three different stages of leakage when measuring current as a function of time: (1) charging, (2) steady-state, which is the true leakage, and (3) breakdown. Failure to measure the true leakage will lead to artificially high values of the leakage. This is especially an issue when using a

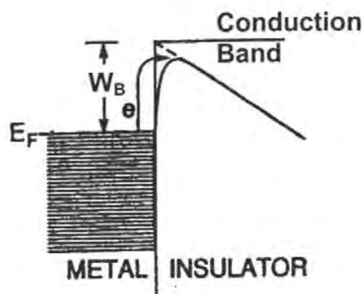

Figure 3-22: Schematic of Schottky emission conduction mechanism.[20]

step or ramp voltage technique and measurements are not taken slowly enough that the current can reach its steady-state leakage value at each voltage.[47] Charging and leakage also have different voltage and temperature dependencies; failure to recognize the difference between the two can give the appearance of different leakage mechanisms operating in different voltage regimes, even though one regime is actually dominated by polarization rather than leakage current.[47]

3.5.2 Leakage Current: $Bi_{1.5}Zn_{1.0}Nb_{1.5}O_7$

The possible mechanisms that dominate charge transfer in BZN may be narrowed through the following observations. First, the thicknesses of the films studied are too large for tunneling between electrodes. Second, an anneal of 500-550 °C for 30-45 s is required after the Pt top electrode sputter deposition to achieve a low loss tangent. Sputtering of electrodes is not expected to cause a change in the bulk of the film, nor is much of a change in the bulk expected for an anneal at these relatively mild temperatures. Third, the leakage shows a dependence on the top electrode material as shown in Figure 3-23. Fourth, a dependence of the leakage on the polarity of the applied voltage is

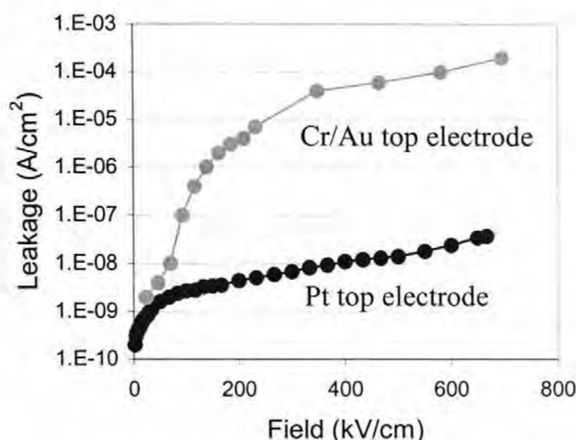

Figure 3-23: Plot of leakage current vs. dc field of samples with either Pt or Cr/Au top electrodes.

observed when the top and bottom electrodes are not the same material. This is revealed in Figure 3-24, since there is noticeably higher leakage when the top electrode is negative. This behavior was not found when both top and bottom electrodes are Pt. These effects can be used as evidence that leakage currents in BZN are interface controlled.[2,34,35,48] However, when different electrodes were used on PLT films ($Pb_{1.19}La_{0.04}TiO_{3.25}$ and $Pb_{1.19}La_{0.05}TiO_{3.27}$) there was also a polarity dependence of leakage when SCLC occurs.[49]

One possible explanation of the difference in properties based upon the top electrode material is that Pt and Cr/Au electrodes have different work functions, 5.7 eV for Pt, 4.8 eV for Au, and 4.5 eV for Cr.[50] These values are "mid-range" values since a range of values is reported in literature. A work function is the critical energy required for electrons to escape from the metal.[45]

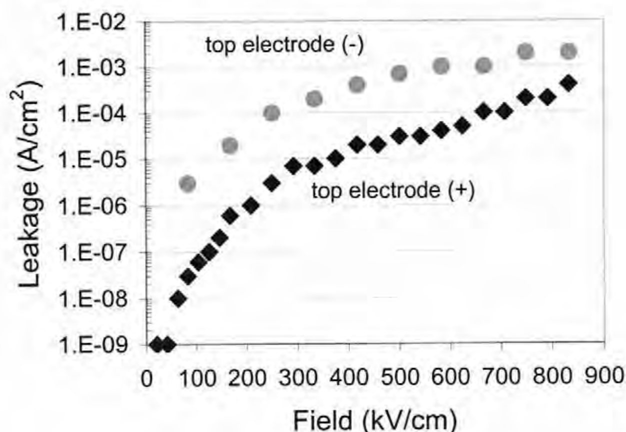

Figure 3-24: Plot of leakage current as a function of applied dc field for 120 nm $Bi_{1.5}Zn_{1.0}Nb_{1.5}O_7$ film with Cr/Au top electrodes.

The third and fourth observations for BZN films described above are similar to those of Dietz et al.,[2] who observed that NiCr/Au as negative electrode resulted in relatively high leakage currents in $SrTiO_3$ compared to the case of NiCr/Au as the positive electrode. In the case of Pt electrodes, Dietz et al. found leakage is low and independent of polarity when Pt is used for both the top and bottom electrodes.[2] It was concluded that the leakage in $SrTiO_3$ films is not space-charge limited but electrode limited.[2]

Although from Figures 3-23 and 3-24 it can be seen that the electrodes control injection, and therefore the amount of leakage, it can be difficult to determine precisely which conduction mechanisms are dominant. For example, determining if SCLC occurs is not straightforward since Equation 3.7 assumes field-independent mobility (μ in Equation 3.7). However, this is not always true, especially at high fields.[39] One possible

reason for this is at high fields, the velocity of carriers increases rapidly with field, leading to a heating of the carriers. It is possible that the leakage of BZN films could be accurately interpreted by modifying Equation 3.7 to include a field dependent mobility. For example, the mobility has been modified to account for constant-mean-free-path considerations at high fields such as deformation potential and acoustic mode scattering.[39]

$Bi_{1.5}Zn_{1.0}Nb_{1.5}O_7$ was found to have thickness independent leakage currents. Figure 3-25 shows the leakage of $Bi_{1.5}Zn_{1.0}Nb_{1.5}O_7$ as a function of thickness. These results are important for use in potential applications such as decoupling capacitors since thinner films are required to increase capacitance. However, the leakage under negative field was not measured, so it is not currently known if a plot showing leakage under both positive and negative voltages is symmetrical.

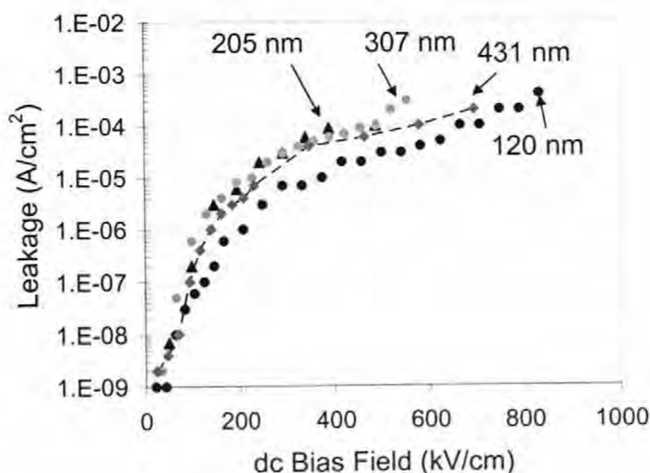

Figure 3-25: Leakage current of varying thicknesses of $Bi_{1.5}Zn_{1.0}Nb_{1.5}O_7$ films with Cr/Au top electrodes, as a function of applied dc field.

3.5.3 Leakage Current: $Bi_{1.5}Zn_{0.5}Nb_{1.5}O_{6.5}$

Figure 3-26 shows the leakage current of $Bi_{1.5}Zn_{0.5}Nb_{1.5}O_{6.5}$ with Pt top electrodes as a function of dc field. Comparing these data to leakage results for $Bi_{1.5}Zn_{1.0}Nb_{1.5}O_7$ with Pt electrodes (Figure 3-23), $Bi_{1.5}Zn_{0.5}Nb_{1.5}O_{6.5}$ would appear to have lower leakage. However, the leakage values for $Bi_{1.5}Zn_{0.5}Nb_{1.5}O_{6.5}$ are comparable to those of $Bi_{1.5}Zn_{1.0}Nb_{1.5}O_7$ measured by Dr. Maria at North Carolina State University. This suggests that there is some sample to sample variability in the leakage values. In general, though, it can be said that the leakage behavior of $Bi_{1.5}Zn_{0.5}Nb_{1.5}O_{6.5}$ is similar to $Bi_{1.5}Zn_{1.0}Nb_{1.5}O_7$.

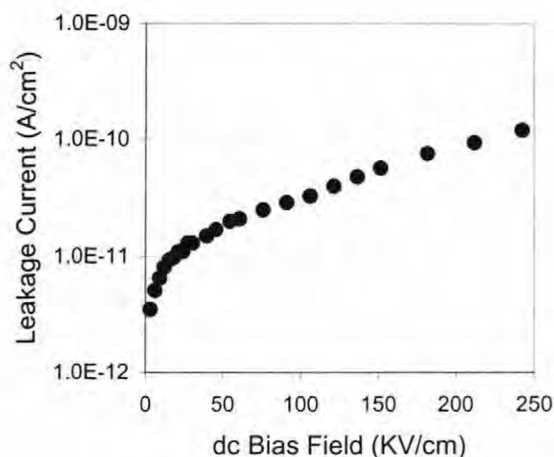

Figure 3-26: Leakage current of $Bi_{1.5}Zn_{0.5}Nb_{1.5}O_{6.5}$ films as a function of applied dc field; Pt top electrodes.

3.6 References

1. W. Ren, S. Trolier-McKinstry, C.A. Randall and T.R. Shrout, "Bismuth Zinc Niobate Pyrochlore Dielectric Thin Films for Capacitive Applications," *J. Appl. Phys.* **89** (1) 767-74 (2001).

2. G.W. Dietz, W. Antpohler, M. Klee and R. Waser, "Electrode Influence on the Charge Transport through $SrTiO_3$ Thin Films," *J. Appl. Phys.* **78** (10) 6113-21 (1995).

3. C. Basceri, S.K. Streiffer, A.I. Kingon and R. Waser, "The Dielectric Response as a Function of Temperature and Film Thickness of Fiber-Textured $(Ba,Sr)TiO_3$ Thin Films Grown by Chemical Vapor Deposition," *J. Appl. Phys.* **82** (5) 2497-504 (1997).

4. J.P. Maria, C.B. Parker, F. Ayguavives, A. Tombak, G.T. Stauf, A. Mortazawi and A.I. Kingon, "Progress in $BaTiO_3$ Thin Films: High Frequency Applications and Property Investigations," *Extended Abstract 10th US-Japan Seminar on Dielectric and Piezoelectric Ceramics* (Providence, RI, 2001) 91-4.

5. T. Kuroiwa, Y. Tsunemine, T. Horikawa, T. Makita, J. Tanimura, N. Mikami and K. Sato, "Dielectric Properties of $(Ba_xSr_{1-x})TiO_3$ Thin Films Prepared by RF Sputtering for Dynamic Random Access Memory Application," *Jpn. J. Appl. Phys.* **33** (Pt. 1, 9B) 5187-91 (1994).

6. J.C. Nino, "Fundamental Structure-Property Relationships Towards Engineering of an Integrated NPO Capacitor for Bismuth Pyrochlore Systems," Ph.D. Thesis, The Pennsylvania State University, 2002.

7. C.-L. Huang, M.-H. Weng and C.-C. Yu, "Low Firable $BiNbO_4$ Based Microwave Dielectric Ceramics," *Ceram. Int.* **27** 343-50 (2001).

8. J.C. Nino, M.T. Lanagan and C.A. Randall, "Dielectric Relaxation in the Bi_2O_3 - ZnO-Nb_2O_5 Cubic Pyrochlore," *J. Appl. Phys.* **89** (8) 4512-5 (2001).

9. S. Kamba, V. Porokhonsky, A. Pashkin, V. Bovtun, J. Petzelt, J.C. Nino, S. Trolier-McKinstry, M.T. Lanagan and C.A. Randall, "Anomalous Broad Dielectric Relaxation in $Bi_{1.5}Zn_{1.0}Nb_{1.5}O_7$ Pyrochlore," *Phys. Rev. B.* **66** (5) 054106/1-8 (2002).

10. D. Viehland, S.J. Jang, L.E. Cross and M. Wuttig, "Freezing of the Polarization Fluctuations in Lead Magnesium Niobate Relaxors," *J. Appl. Phys.* **68** 2916-21 (1990).

11. D. Huser, L.E. Wegner, A.J. van Duyneveldt and J.A. Mydosh, "Dynamical Behavior of the Susceptibility Around the Freezing Temperature in (Eu,Sr)S," *Phys. Rev. B* **27** 3100-3 (1983).

12. E. Courtens, "Vogel-Fulcher Scaling of the Susceptibility in a Mixed-Crystal Proton Glass," *Phys. Rev. Lett.* **52** 69-72 (1984).

13. W.J. Kim, W. Chang, S.B. Qadri, J.M. Pond, S.W. Kirchoefer, D.B. Chrisey and J.S. Horwitz, "Microwave Properties of Tetragonally Distorted $(Ba_{0.5}Sr_{0.5})TiO_3$ Thin Films," *Appl. Phys. Lett.* **76** (9) 1185-7 (2000).

14. I. Levin, T.G. Amos, J.C. Nino, T.A. Venderah, I.M. Reaney, C.A. Randall and M.T. Lanagan, "Crystal Structure of the Compound $Bi_2Zn_{2/3}Nb_{4/3}O_7$," *Mat. Res. Bull.* **17** (6) 1406-11 (2002).

15. R. Waser, "Modeling of Electroceramics – Applications and Prospects," *J. Eur. Ceram. Soc.* **19** 655-64 (1999).

16. A.E. Glazounov and A.K. Tagantsev, "Crossover in a Non-Analytical Behavior of Dielectric Non-Linearity in $PbMn_{1/3}Nb_{2/3}O_3$ Relaxor Ferroelectrics," *J. Phys.: Condens. Matter* **10** 8863-80 (1998).

17. E.V. Colla, S.M. Gupta and D. Viehland, "Alternating Current Field Effect on the Freezing Temperature of Relaxor Ferroelectrics," *J. Appl. Phys.* **85** (1) 362-7 (1999).

18. H.N. Al-Shareef, K.R. Bellur, O. Auciello and A.I. Kingon, "Phase Evolution and Annealing Effects on the Electrical Properties of $Pb(Zr_{0.53}Ti_{0.47})O_3$ Thin Films with RuO_2 Electrodes," *Thin Solid Films* **256** 73-9 (1995).

19. L.D. Smith, R.E. Anderson, D.W. Forehand, T.J. Pelc and T. Roy, "Power Distribution System Design Methodology and Capacitor Selection for Modern CMOS Technology," *IEEE Trans. on Adv. Packag.* **22** (3) 284-91 (1999).

20. M. Ohring, *The Materials Science of Thin Films* (Academic Press, San Diego, 1992).

21. P.C. Joshi and S.B. Krupanidhi, "Structural and Electrical Characteristics of $SrTiO_3$ Thin Films for Dynamic Random Access Memory Applications," *J. Appl. Phys.*, **73** (11) 7627-34 (1993).

22. G.R. Fox and S.B. Krupanidhi, "Nonlinear Electrical Properties of Lead-Lanthanum-Titanate Thin Films Deposited by Multi-Ion-Beam Reactive Sputtering," *J. Appl. Phys.* **74** (3) 1949-59 (1993).

23. A.K. Jonscher and R.M. Hill, *Physics of Thin Films*, Vol. 8 (Academic Press, 1975).

24. J.F. Scott, C.A. Paz de Auraujo, B.M. Melnick, L.D. McMillan and R. Zuleeg, "Quantitative Measurement of Space-Charge Effects in Lead Zirconate-Titanate Memories," *J. Appl. Phys.* **70** (1) 382-8 (1991).

25. P.C. Joshi and S.B. Krupanidhi, "Strontium Titanate Thin Films by Rapid Thermal Processing," *Appl. Phys. Lett.* **61** (13) 1525-7 (1992).

26. K. Abe and S. Komatsu, "Epitaxial-Growth of $SrTiO_3$ Films on Pt Electrodes and Their Electrical Properties," *Jpn. J. Appl. Phys.*, 1 **31** (9B) 2985-8 (1992).

27. R. Moazzami, C.M. Hu and W.H. Shepherd, "Electrical Characteristics of Ferroelectric PZT Thin-Films for DRAM Applications," *IEEE Trans. Electron Devices* **39** (9) 2044-9 (1992).

28. K. Abe and S. Komatsu, "Dielectric Constant and Leakage Current of Epitaxially Grown and Polycrystalline $SrTiO_3$ Thin-Films," *Jpn. J. Appl. Phys.* 1 **32** (9B) 4186-9 (1993).

29. W. Antpohler, G.W. Dietz, M. Klee and R. Waser, *Proceedings of the Electroceramics IV* (Augustinus, Aachen, 1994), pp.169-72.

30. D.J. Wouters, G. Willems, G. Groeneseken, H.E. Maes and K. Brooks, "Elements of the Leakage Current of High-Epsilon Ferroelectric PZT Films," *Integr. Ferroelectr.* **7** (1-4) 173-84 (1995).

31. H. Hu and S.B. Krupanidhi, "Current-Voltage Characteristics of Ultrafine-Grained Ferroelectric $Pb(Zr,Ti)O_3$ Thin Films," *J. Mater. Res.* **9** (6) 1484-98 (1994).

32. Y. Fukuda, K. Aoki, K. Numata and A. Nishimura, "Current-Voltage Characteristics of Electron-Cyclotron-Resonance Sputter-Deposited $SrTiO_3$," *Jpn. J. Appl. Phys.*, 1 **33** (9B) 5255-8 (1994).

33. T. Tamura, K. Takai, H. Noshiro, M. Kimura, S. Otani and M. Yamada, "Influence of Electrode Contacts on Leakage Current of $SrTiO_3$ Capacitors," *Jpn. J. Appl. Phys.*, 2 **33** (12A) L1697-9 (1994).

34. J.J. Lee, C.L. Thio and S.B. Desu, "Electrode Contacts on Ferroelectric $Pb(Zr_x Ti_{1-x})O_3$ and $SrBi_2Ta_2O_9$ Thin Films and their Influence on Fatigue Properties," *J. Appl. Phys.* **78** (8) 5073-8 (1995).

35. R. Waser, in *Science and Technology of Electroceramic Thin Films*, edited by O. Auciello and R. Waser (Kluwer, Dordrecht, 1995), pp. 23-248.

36. G.W. Dietz, M. Schumacher, R. Waser, S.K. Streiffer, C. Basceri and A.I. Kingon, "Leakage Currents in $Ba_{0.7}Sr_{0.3}TiO_3$ Thin Films for Ultrahigh-Density Dynamic Random Access Memories," *J. Appl. Phys.* **82** (5) 2359-64 (1997), and references cited therein.

37. S.M. Sze, *Physics of Semiconductor Devices* (Wiley, New York, 1981).

38. K.C. Kao and W. Hwang, *Electrical Transport in Solids* (Pergamon, New York, 1981).

39. M.A. Lampert and P. Mark, *Current Injection in Solids* (Academic, New York, 1970).

40. J.J. O'Dwyer, *The Theory of Electrical Conduction and Breakdown in Solid Dielectrics* (Clarendon, Oxford, 1973).

41. J.G. Simmons, "Potential Barriers and Emission-Limited Current Flow Between Closely Spaced Parallel Metal Electrodes," *J. Appl. Phys.* **35** (8) 2472-81 (1964).

42. J.G. Simmons, "Poole-Frenkel Effect and Schottky Effect in Metal-Insulator-Metal Systems," *Phys. Rev.* **155** (3) 657-60 (1967).

43. J.G. Simmons, "Transition from Electrode-Limited to Bulk-Limited Conduction Processes in Metal-Insulator-Metal Systems," *Phys. Rev.* **166** (3) 912-20 (1968).

44. J.G. Simmons, "Theory of Metallic Contacts on High Resistivity Soilds – I. Shallow Traps," *J. Phys. Chem. Solids* **32** 1987-99 (1971); "Theory of Metallic Contacts on High Resistivity Soilds – II. Deep Traps," *J. Phys. Chem. Solids* **32** 2581-91 (1971).

45. L. Solymer and D. Walsh, *Lectures on the Electrical Properties of Materials* (Oxford Science Publications, Oxford, 1995).

46. I. Stolichnov, A.K. Tagantsev, E.L. Colla, and N. Setter, "Cold-Field-Emission Test of the Fatigued State of $Pb(Zr_xTi_{1-x})O_3$ Films," *Appl. Phys. Lett.* **73** (10) 1361-3 (1998).

47. C. Basceri, "Electrical and Dielectric Properties of $(Ba,Sr)TiO_3$ Thin Film Capacitors for Ultra-High Density Dynamic Random Access Memories," Ph.D. Thesis, North Carolina State University, 1997.

48. R. Waser, "Dielectric Analysis of Integrated Ceramic Thin Film Capacitors," *Integr. Ferroelectr.* **15** (1-4) 39-51 (1997), and references cited therein.

49. G.R. Fox, "Composition/Structure/Property Relations of Ferroelectric Lead-Lanthanum-Titanate Thin Films Deposited by Multi-Ion-Beam Reactive Sputtering," Ph.D. Thesis, The Pennsylvania State University, 1992.

50. W.R. Runyan and K.E. Bean, *Semiconductor Integrated Circuit Processing Technology* (Addison Wesley, Reading, MA, 1990).

Chapter 4

SUMMARY AND FUTURE WORK

4.1 Summary

In this thesis, three compositions of BZN thin films were studied: $Bi_{1.5}Zn_{1.0}Nb_{1.5}O_7$, $Bi_2Zn_{2/3}Nb_{4/3}O_7$, and $Bi_{1.5}Zn_{0.5}Nb_{1.5}O_{6.5}$. Possible applications include tunable filter applications due to the high permittivity, low TCC, and tunability of the permittivity. Another potential application is on-chip decoupling capacitors, due to these properties and the relatively low processing temperatures of BZN films.

Figure 4-1 shows a ternary composition diagram illustrating the relationship of the three compositions of BZN films studied. Similarities in properties between $Bi_{1.5}Zn_{1.0}Nb_{1.5}O_7$ and $Bi_{1.5}Zn_{0.5}Nb_{1.5}O_{6.5}$ are due to their similar structure and compositions. The fact that $Bi_{1.5}Zn_{0.5}Nb_{1.5}O_{6.5}$ decomposes at 700 °C into cubic BZN and $BiNbO_4$ can be explained since $Bi_{1.5}Zn_{0.5}Nb_{1.5}O_{6.5}$ lies along the tie line connecting $Bi_{1.5}Zn_{1.0}Nb_{1.5}O_7$ and $BiNbO_4$.

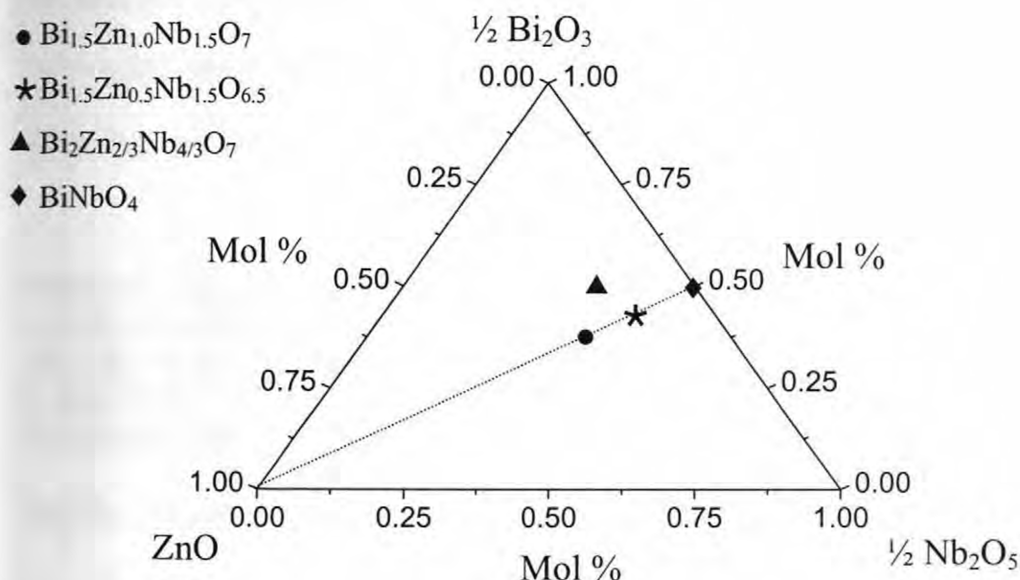

Figure 4-1: Ternary composition diagram for the Bi_2O_3 – ZnO – Nb_2O_5 system. Also shown is the tie line relating ZnO, $Bi_{1.5}Zn_{1.0}Nb_{1.5}O_7$, $Bi_{1.5}Zn_{0.5}Nb_{1.5}O_{6.5}$, and $BiNbO_4$.

It was found that when compared with $Bi_{1.5}Zn_{1.0}Nb_{1.5}O_7$, $Bi_{1.5}Zn_{0.5}Nb_{1.5}O_{6.5}$ shows some similarities and some important differences. Both compositions crystallize at 550 °C into the cubic pyrochlore structure, have processing temperature dependent dielectric properties, negative TCC, similar loss tangents (< 0.005), and show similar tunability (~ 26 % at 1.8 MV/cm). However, $Bi_{1.5}Zn_{0.5}Nb_{1.5}O_{6.5}$ has a higher permittivity (180 vs. 150 for $Bi_{1.5}Zn_{1.0}Nb_{1.5}O_7$), lower processing temperatures to obtain the maximum permittivity (600 °C vs. 750 °C), and smaller TCC (-275 ppm/°C vs. -400 ppm/°C). It was suggested that the amount of Zn affects the occupancy on the A-site as opposed to forming a ZnO second phase. Both $Bi_{1.5}Zn_{1.0}Nb_{1.5}O_7$ and $Bi_2Zn_{2/3}Nb_{4/3}O_7$ thin films have dielectric properties comparable to bulk values;[1] however

$Bi_{1.5}Zn_{0.5}Nb_{1.5}O_{6.5}$ cannot be compared to bulk ceramics of the same composition since bulk ceramics have not been prepared.[2] A comparison between some properties of BZN films and BZN ceramics is shown in Table 4-1.

Table 4-1: Summary of dielectric properties and processing temperatures for three compositions of BZN, comparing thin film and ceramics. Note that to date, $Bi_{1.5}Zn_{0.5}Nb_{1.5}O_{6.5}$ ceramic samples were not prepared.[2]

Composition		ε_r	tanδ	TCC	Processing Temperature
$Bi_2Zn_{2/3}Nb_{4/3}O_7$	thin film[1]	82	< 0.005	150 ppm/°C	750 °C
	ceramics[2]	81	< 0.001	170 ppm/°C	950 °C
$Bi_{1.5}Zn_{1.0}Nb_{1.5}O_7$	thin film[1]	150	< 0.005	-400 ppm/°C	750 °C
	ceramics[2]	145	< 0.005	-390 ppm/°C	950 °C
$Bi_{1.5}Zn_{0.5}Nb_{1.5}O_{6.5}$	thin film	180	< 0.005	-270 ppm/°C	600 – 650 °C
	ceramics	--	--	--	--

Figure 4-2 shows two experimentally determined composition diagrams that are possible for the BZN system. Each represents the tie line shown in Figure 4-1 between ZnO and $BiNbO_4$, and combines results from ceramics and thin films. Since two thin film cubic BZN compositions were tested in this thesis, the additional information necessary to generate this phase diagram was reported by Nino.[2] In the case of thin films, the cubic pyrochlore structure forms for $Bi_{1.5}Zn_{1.0}Nb_{1.5}O_7$ and $Bi_{1.5}Zn_{0.5}Nb_{1.5}O_{6.5}$; however, the actual composition range in which cubic BZN forms is not known and is therefore represented in Figure 4-2 as dashed lines. Cubic BZN formed at temperatures as low as 550 °C for MOD thin films, which is lower than the temperatures Nino studied for BZN ceramics.[2]

Nino found that BZN ceramics with Zn = 0.5 formed cubic BZN and $BiNbO_4$.[2] However, higher processing temperatures were used for ceramics than for thin films. In the case of thin films, $Bi_{1.5}Zn_{0.5}Nb_{1.5}O_{6.5}$ processed between 550 and 650 °C forms cubic BZN with no $BiNbO_4$ detected. The presence of cubic pyrochlore for $Bi_{1.5}Zn_{0.5}Nb_{1.5}O_{6.5}$ in thin films but not in ceramics is believed to be due to the different kinetics in thin film crystallization compared with bulk ceramics. Little is known about the phase(s) present in Region 1 in Figure 4-2a.

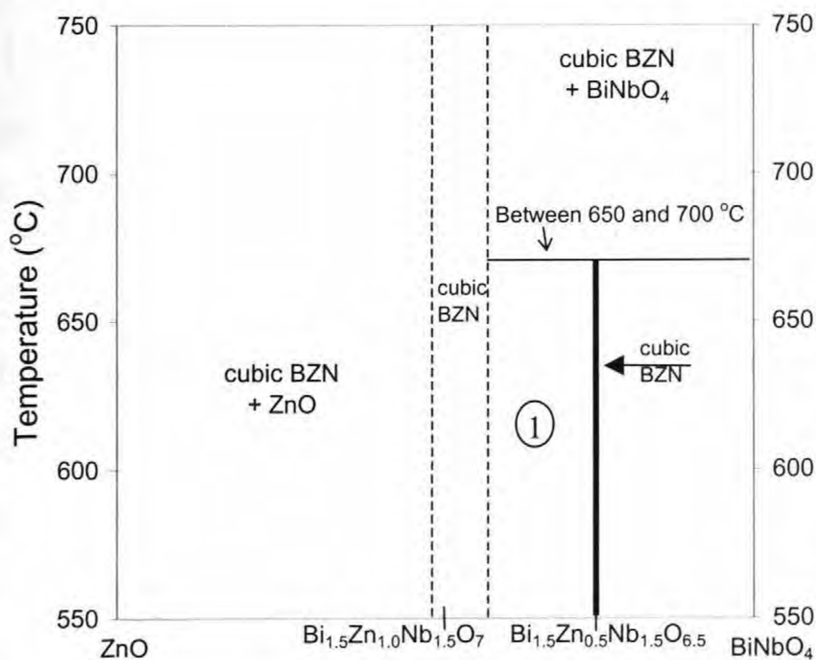

Figure 4-2a: A possible phase diagram for the BZN system combining experimentally determined thin film and ceramic data.

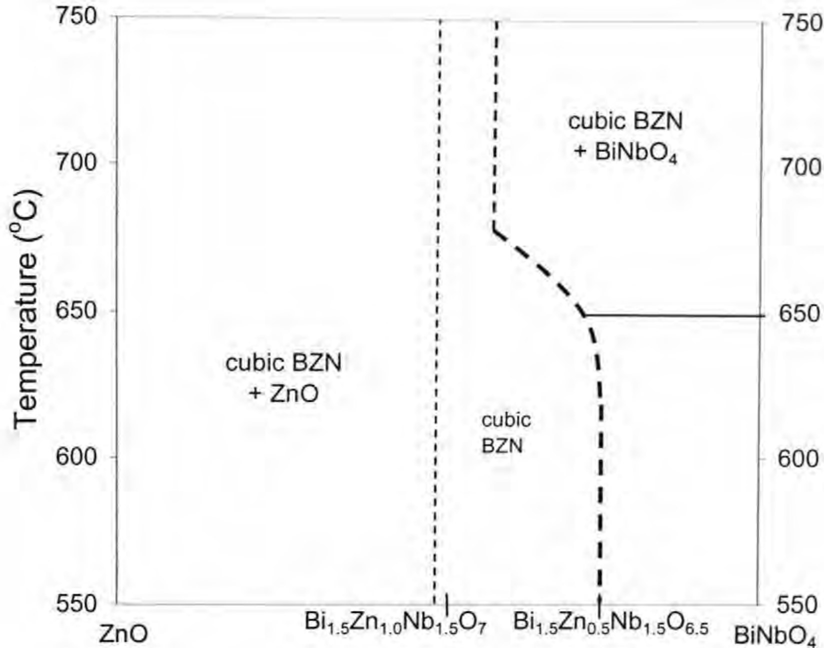

Figure 4-2b: A possible phase diagram for the BZN system combining experimentally determined thin film and ceramic data.

Both $Bi_{1.5}Zn_{1.0}Nb_{1.5}O_7$ and $Bi_{1.5}Zn_{0.5}Nb_{1.5}O_{6.5}$ show similar behavior in the tunability of the permittivity. The maximum tunability of $Bi_{1.5}Zn_{1.0}Nb_{1.5}O_7$ was measured to be 45 % at 3.0 MV/cm. In addition, it was found that the permittivity of $Bi_2Zn_{2/3}Nb_{4/3}O_7$ is tunable at high dc fields with 20 % maximum tunability at 4.0 MV/cm. The fact that the permittivity increases, then decreases with field is attributed to field-induced ordering of Zn atoms within the hexagonal tungsten bronze layer in the zirconolite structure.[3]

In this thesis, it was shown that $Bi_{1.5}Zn_{1.0}Nb_{1.5}O_7$ films have thickness-independent dielectric properties down to a thickness of 520 Angstroms. Permittivity and loss tangent, as well as dc field tunability, showed thickness independent behavior. It

was also found that for a 520 Angstroms BZN film, the equivalent oxide thickness of 14.4 Angstroms is twice as thick as for BST at the same thickness.

It was found that BZN films are tunable with ac electric fields. The permittivity of cubic and monoclinic compositions increased with applied ac field, although by different amounts: < 1 % for $Bi_2Zn_{2/3}Nb_{4/3}O_7$ at 500 kV/cm, as opposed to 6 % for $Bi_{1.5}Zn_{0.5}Nb_{1.5}O_{6.5}$ at the same field. Since the permittivity of BZN films increases with ac field but decreases with dc field, it can be concluded that different mechanisms are responsible for the two phenomena. Again, higher ac field data are necessary since under relatively low dc fields, the permittivity of $Bi_2Zn_{2/3}Nb_{4/3}O_7$ also increases to a maximum.

The dielectric relaxation of cubic $Bi_{1.5}Zn_{0.5}Nb_{1.5}O_{6.5}$ was analyzed, and it was found that it is similar to $Bi_{1.5}Zn_{1.0}Nb_{1.5}O_7$, with an activation energy and jump frequency calculated from an Arrhenius relation of 0.11 ± 0.0054 eV and $4.57 \times 10^{12} \pm 2.86$ Hz, respectively. These values are reasonable since they are comparable to those reported for $Bi_{1.5}Zn_{1.0}Nb_{1.5}O_7$ thin films[1] and $Bi_{1.5}Zn_{1.0}Nb_{1.5}O_7$ ceramics by Nino[2] and Kamba.[4] However, the onset of relaxation occurred ~30-50 K lower than in $Bi_{1.5}Zn_{1.0}Nb_{1.5}O_7$ and the maximum in loss tangent peak was lower magnitude. This is important for applications since higher frequencies can be reached without the loss tangent increasing due to the dielectric relaxation.

Through studying the relaxation of cubic BZN, it can be concluded that the currently predominant models of ferroelectric relaxors described in Chapter 1 are not applicable to BZN. For example, models such as superparaelectric and dipole glass would predict similar tunability behavior for both ac and dc fields.[5] However, this thesis

has shown that the permittivity decreases under dc field and increases under ac field. The breathing model proposed by Glazounov and Tagantsev predicts these differing behaviors for PMN.[5] However, it is not clear what the corollary is to domain wall motion and spontaneous polarization, since BZN is not ferroelectric. However, the model of relaxation proposed by Nino for BZN ceramics[2] may also apply to BZN thin films. It attributes the relaxation to a jump from one energy potential well to another over an energy barrier associated with the activation energy calculated from the Arrhenius behavior. Within each energy well, there are smaller jumps possible due to multiple states that are thermodynamically equivalent. These smaller jumps are dictated by random fields that result from phenomena such as site disorder.[2]

Leakage currents of BZN films were also measured. It was found that $Bi_{1.5}Zn_{1.0}Nb_{1.5}O_7$ and $Bi_{1.5}Zn_{0.5}Nb_{1.5}O_{6.5}$ have low leakage. It was also found that $Bi_{1.5}Zn_{1.0}Nb_{1.5}O_7$ has thickness independent leakage for films ~50 nm and above.

4.2 Future Work

This thesis has explored parameters such as composition, effects of ac and dc fields, and leakage to reveal underlying behaviors that affect the properties of BZN films. These behaviors can be further explored through experiments described below.

As mentioned in various places throughout this thesis, thinner films would be useful to examine whether or not properties such as leakage and permittivity are thickness independent at thicknesses smaller than 500 Angstroms. A technological advantage to thinner films is the capacitance per area increases, which is useful for

applications such as decoupling capacitors. Thinner films are also advantageous for tunable applications, since lower voltages are required to obtain specific fields. Thinner films can be achieved by diluting the MOD solution to reduce its concentration before spin coating, by treating the surface of the substrates to increase wetting, or by using a different thin film deposition method.

It would also be useful to measure the dielectric properties of BZN films under higher fields, both ac and dc, than were used in this thesis. For example, the mechanism responsible for ac tunability of BZN films might be clarified through these measurements. The accuracy of the higher order terms of polarization as a function of voltage can be improved, and a useful equation to fit ac tunability data might be found.

The behavior of BZN films at higher frequencies is also worth examining. Since dielectric properties of BZN films are similar to those of BZN ceramics, it would be beneficial to see if the similarities continue into the high frequency regime. Some techniques that were used for BZN ceramics include time domain transmission THz spectroscopy (90 – 900 GHz), and infrared spectroscopy (0.6 – 100 THz).[4] In addition to measuring the permittivity as a function of frequency, the behavior of the permittivity of BZN films under high fields has not been studied at high frequencies. These data would be very applicable for high frequency applications since some operate under an applied voltage.

It would be important to measure the loss tangent as a function of both temperature and frequency in cubic BZN films. Following the work of Nino[2] on bulk BZN ceramics, a similar study can be conducted for BZN films in order to accurately

model the dielectric relaxation in cubic BZN. In addition to studying the relaxation as a function of temperature and frequency, including field as another parameter would improve the relaxation model.

Another area of focus worthy of further study is developing the BZN phase diagram more precisely. One method would be to vary the composition in order to explore the limits of cubic BZN formation. This will have to be done as a function of temperature also, since cubic BZN is even detected in $Bi_2Zn_{2/3}Nb_{4/3}O_7$ at a processing temperature of 550 °C to 700 °C, but only monoclinic BZN is present at 750 °C.[1] An especially useful set of experiments would vary the amount of Zn in cubic BZN to determine the phases present in Region 1 of Figure 4-2a, between $Bi_{1.5}Zn_{1.0}Nb_{1.5}O_7$ and $Bi_{1.5}Zn_{0.5}Nb_{1.5}O_{6.5}$. It would also be useful to measure the dielectric properties of $Bi_{1.5}Zn_{0.92}Nb_{1.5}O_{6.92}$, since this composition is phase-pure for ceramics.[2] These data would reveal more information about the role of structure and composition on properties of cubic BZN.

The microstructure and phase development of BZN films can be examined in a number of ways. One set of experiments that could be used in an attempt to lower the crystallization temperature for BZN films is to anneal the films for significantly longer times than used in this thesis (an example is on the order of tens of hours, as opposed to two minutes used in this thesis). This could lead to films crystallizing at lower temperatures than reported thus far. In addition, TEM could be used to study the microstructure of BZN films processed under different conditions (for example, different processing temperatures) to reveal the correlation between microstructure and properties.

The crystallization behavior of BZN films can be studied by constructing T-T-T (time-temperature-transformation) curves. Crystallization is plotted as a function of temperature and time, and can be analyzed to determine the nucleation and growth behavior of the crystalline phase. In addition, TEM can also be used to examine BZN films to determine if there is any residual amorphous phase in crystalline films. For example, it would be interesting to study whether the dependence of the dielectric properties on crystallization temperature is due to the presence of an amorphous phase which decreases with increasing processing temperature.

The conduction mechanisms that occur in BZN films can be studied in a number of ways. One set of measurements that would yield very useful results would be to measure the leakage current as a function of temperature. The temperature dependence, if present, would be useful in narrowing the number of conduction mechanisms. Another technique that can be used to explore conduction mechanisms in BZN films is measurement of the effect of photo-excitation on leakage current. For example, monochromatic light could excite carriers from shallow traps into the conduction band. By varying the wavelength of light and measuring the leakage, it could be determined at what wavelength carriers are excited into the conduction band. This would lead to a better understanding of the trap depth in BZN films.

Conclusions and hypotheses drawn from BZN films could be verified by synthesizing and characterizing additional Bi-pyrochlore films. For example, Cann found that $Bi_{1.5}Mg_{1.0}Nb_{1.5}O_7$ ceramics have a higher permittivity than BZN ceramics, while $Bi_{1.5}Zn_{1.0}Ta_{1.5}O_7$ ceramics have lower loss tangent.[6] Characterizing new compositions of

both BZT and BMN would be useful since through decreasing the amount of Zn in cubic BZN the permittivity increased, TCC was smaller, and the dielectric relaxation occurred at lower temperatures. For example, the dielectric properties of $Bi_{1.5}Zn_{0.5}Ta_{1.5}O_{6.5}$ might show a higher permittivity and different TCC than $Bi_{1.5}Zn_{1.0}Ta_{1.5}O_7$ using the descriptions included in this thesis for BZN films.

4.3 References

1. W. Ren, S. Trolier-McKinstry, C.A. Randall and T.R. Shrout, "Bismuth Zinc Niobate Pyrochlore Dielectric Thin Films for Capacitive Applications," *J. Appl. Phys.* **89** (1) 767-74 (2001).

2. J.C. Nino, "Fundamental Structure-Property Relationships Towards Engineering of an Integrated NPO Capacitor for Bismuth Pyrochlore Systems," Ph.D. Thesis, The Pennsylvania State University, 2002.

3. I. Levin, T.G. Amos, J.C. Nino, T.A. Venderah, I.M. Reaney, C.A. Randall and M.T. Lanagan, "Crystal Structure of the Compound $Bi_2Zn_{2/3}Nb_{4/3}O_7$," *Mat. Res. Bull.* **17** (6) 1406-11 (2002).

4. S. Kamba, V. Porokhonsky, A. Pashkin, V. Bovtun, J. Petzelt, J.C. Nino, S. Trolier-McKinstry, M.T. Lanagan and C.A. Randall, "Anomalous Broad Dielectric Relaxation in $Bi_{1.5}Zn_{1.0}Nb_{1.5}O_7$ Pyrochlore," *Phys. Rev. B.* **66** (5) 054106/1-8 (2002).

5. A.E. Glazounov and A.K. Tagantsev, "Crossover in a Non-Analytical Behavior of Dielectric Non-Linearity in $PbMn_{1/3}Nb_{2/3}O_3$ Relaxor Ferroelectrics," *J. Phys.: Condens. Matter* **10** 8863-80 (1998).

6. D.P. Cann, "Bismuth Pyrochlores for High Frequency Dielectric Applications," M.S. Thesis, The Pennsylvania State University, 1993.